DMM Advance Online Articles. Posted 3 March 2016 as doi: 10.1242/dmm.022939
Access the most recent version at http://dmm.biologists.org/lookup/doi/10.1242/dmm.022939

Neurological Roles for Phosphomannomutase Type 2 in a New *Drosophila* Congenital Disorder of Glycosylation Disease Model

William M. Parkinson[1], Michelle Dookwah[4], Mary Lynn Dear[1], Cheryl L. Gatto[1,3], Kazuhiro Aoki[5], Michael Tiemeyer[4,5] and Kendal Broadie[1,2,3*]

Department of Biological Sciences[1], Department of Cell and Developmental Biology[2], Kennedy Center for Research on Human Development[3], Vanderbilt University, Nashville, TN 37235 USA

Department of Biochemistry and Molecular Biology[4], Complex Carbohydrate Research Center[5], The University of Georgia, Athens, GA 30602 USA

Key Words: synapse, neurotransmission, neuromuscular junction, synaptomatrix, matrix metalloproteinase, Wnt, *trans*-synaptic signaling

*Corresponding author email: kendal.broadie@vanderbilt.edu

Summary Statement

This work generates a new *Drosophila* congenital disorder of glycosylation model for the most common disease category, caused by phosphomannomutase-2 mutation, and reveals a synaptic mechanism underlying associated neurological impairments.

Abstract

Congenital disorders of glycosylation (CDGs) constitute a rapidly growing family of human diseases resulting from heritable mutations in genes driving production and modification of glycoproteins. The resulting symptomatic hypoglycosylation causes multisystemic defects that include severe neurological impairments, revealing a particularly critical requirement for tightly regulated glycosylation in the nervous system. The most common CDG, CDG-Ia or PMM2-CDG, arises from phosphomannomutase type 2 (PMM2) mutations. Here, we report the generation and characterization of the first *Drosophila* PMM2-CDG model. CRISPR-generated *Drosophila pmm2* null mutants display severely disrupted glycosylation and early lethality, while RNAi-targeted neuronal PMM2 knockdown results in a strong shift in pauci-mannose glycan abundance, progressive incoordination and later lethality, closely paralleling human CDG-Ia symptoms of shortened lifespan, movement impairments and defective neural development. Analyses of the well-characterized *Drosophila* neuromuscular junction (NMJ) reveal synaptic glycosylation loss accompanied by structural architecture and functional neurotransmission defects. NMJ synaptogenesis is driven by intercellular signals traversing an extracellular synaptomatrix co-regulated by glycosylation and matrix metalloproteinases (MMPs). Specifically, Wnt Wingless (Wg) *trans*-synaptic signaling depends on the heparan sulfate proteoglycan (HSPG) co-receptor Dally-like protein (Dlp), which is regulated by synaptic MMP activity. Loss of synaptic MMP2, Wg ligand, Dlp co-receptor and downstream *trans*-synaptic signaling occurs with PMM2 knockdown.. Taken together, this *Drosophila* CDG disease model provides a new avenue for the dissection of cellular and molecular mechanisms underlying neurological impairments and a means to discover and test novel therapeutic treatment strategies.

Introduction

Congenital disorders of glycosylation (CDGs) caused by mutation of genes encoding glycosylation pathway proteins are classified into two categories (Freeze et al., 2015): CDG-I disease states include defects in carbohydrate production, lipid-linked oligosaccharide (LLO) formation and attachment of glycan chains to amino acids; CDG-II disease states include defects in modification/maturation of glycan chains after protein attachment. The most common CDG is a CDG-I, called CDG-Ia or PMM2-CDG, resulting from mutations in phosphomannomutase 2 (PMM2) converting mannose-6-phosphate to mannose-1-phosphate, the obligatory precursor for GDP-mannose production and N-linked glycosylation (Andreotti et al., 2014; Freeze et al., 2014; Freeze et al., 2015). Since the first patient in 1980, >100 different mutations in >1000 CDG-Ia patients have been characterized (Freeze et al., 2014; Haeuptle and Hennet, 2009; Jaeken, 2013; Jaeken et al., 1980; Yuste-Checa et al., 2015). CDG-Ia infant mortality is ~20% in the first year, with patients manifesting subsequent increased susceptibility to organ failure, infection and injury (Grunewald, 2009). CDG-Ia patients present with a spectrum of neurological symptoms (Jaeken, 2013), ranging from severe neurological impairments with early death, to mild defects with slight psychomotor delay (Grunewald, 2009; Marquardt and Denecke, 2003). To date, no effective treatments are available, with the only treatment option being symptom management (Grunewald, 2009; Monin et al., 2014; Stefanits et al., 2014).

CDG-Ia modeling is critical for molecular and cellular studies. The initial mouse PMM2 knockout model has been of limited use owing to early embryonic lethality (Thiel et. al., 2006). Heteroallelic combination of two PMM2 mutations allows partial enzymatic activity, protracted embryonic survival and has demonstrated potential maternal dietary intervention in treatment (Schneider et al., 2011). Increased lifespan occurred with mannose feeding prenatally and during gestation, reportedly allowing offspring to develop past critical

periods of PMM2-dependent glycan requirement (Schneider et al., 2011; Thiel et al., 2006). Unfortunately, these results have thus far not been successfully replicated in patient trials, where postnatal oral and intravenous mannose administration failed to improve serum protein glycosylation levels (Kjaergaard et al., 1998; Mayatepek and Kohlmuller, 1998). A subsequent zebrafish model established via PMM2 morpholino knockdown revealed increased motor neuron number, altered cranial development, reduced motility and altered glycan profiles (Cline et al., 2012). Most recently, a similar *Xenopus* morpholino knockdown model demonstrated strong reduction in Wnt signaling, revealing a PMM2 requirement in intercellular communication (Himmelreich et al., 2015). These models have been valuable, but have limitations of morpholino-based approaches with inadequate targeting and concerns about the temporal maintenance of knockdown (Schulte-Merker and Stainier, 2014). We therefore set out to develop a *Drosophila* PMM2-CDG disease model.

The *Drosophila* genome encodes >70% of human disease genes (Reiter et al., 2001), including most linked to glycan-related disorders (Dani et al., 2012; Dani et al., 2014). The human N-linked glycome is more expansive, with higher levels of complex and hybrid branched forms (Katoh and Tiemeyer, 2013), but the N-glycosylation pathway is very highly conserved, with well-mapped glycan profiles and the *Drosophila* genetic toolkit allowing sophisticated manipulation (Altmann et al., 2001; Sarkar et al., 2006). For neurological impairments (Freeze, 2006; Freeze et al., 2015; Jaeken, 2013; Martin, 2003), *Drosophila* provides a host of anatomical, electrophysiological and behavioral assays for neural development and function (Dani el al., 2014; Gatto and Broadie, 2011; Jumbo-Lucioni et al., 2014; Parkinson et al., 2013). In particular, our glycomic RNAi screen uncovered a common role for glycosylation restricting the structure and function of the neuromuscular junction (NMJ) synapse (Dani et al., 2012). Subsequent work on screen hits, including heparan sulfate proteoglycan (HSPG) sulfotranserase (*hs6st*)/sulfatase (*sulf1*), UDP-GlcNAc:α-3-D-

mannoside-β1,2-N-acetylglucosaminyl-transferase I (*mgat1*), α-N-acetylgalactosaminyltransferase (*pgant*), galactose-1-phosphate uridyl-transferase (*galt*) and related pathways (Dani et al., 2012; Dani et al., 2014; Jumbo-Lucioni et al., 2014; Parkinson et al., 2013), has shown disruption of *trans*-synaptic signaling to be a common root cause of the compromised NMJ synaptogenesis underlying movement phenotypes.

In this study, we generate a *Drosophila* CDG-Ia disease model. We show that *Drosophila pmm2* is highly conserved and manipulate gene function by making mutants with CRISPR/Cas9 genome editing and tissue-targeted transgenic RNAi. As in human CDG-Ia patients, *Drosophila pmm2* loss-of-function (LOF) mutants exhibit reduced lifespan and psychomotor retardation proportional to the degree of PMM2 reduction. We show striking impacts on the N-linked glycome: globally in null mutants, neurally in tissue-targeted RNAi knockdown and locally at the NMJ synapse. At the NMJ, targeted pre- and postsynaptic PMM2 knockdown reveals architectural overelaboration, and concurrent reduction on both sides of the synapse strongly increases neurotransmission strength. PMM2 loss strongly impairs the synaptic matrix metalloproteinase (MMP) pathway regulating HSPG co-receptor Dally-like protein (Dlp) to modulate Wnt Wingless (Wg) *trans*-synaptic signaling (Dani et al., 2012; Dear et al., 2016; Freidman et al., 2013). Consistently, PMM2 knockdown reduces Wg, Dlp and the Frizzled Nuclear Import (FNI) pathway. These results suggest a PMM2-dependent extracellular proteinase mechanism modulates Wnt signaling during NMJ synaptogenesis, which underlies coordinated movement and maintained viability. This new *Drosophila* model should lead to novel therapeutic treatments for CDG-Ia.

Results

Degree of *Drosophila PMM2* loss determines lifespan duration

Human *pmm2* contains 8 exons compared to the *Drosophila* CG10688 *pmm2* single reading frame (Fig. 1A), making genetic manipulation and expression studies more amenable. Simplified site-directed CRISPR mutagenesis targeted at one exon reduces the possibility of truncated exons maintaining partial function. Human PMM2 contains 12 active sites that coordinately bind the substrate, mannose-6-phosphate, and convert it to mannose-1-phosphate (Andreotti et al., 2014; Silvaggi et al., 2006). *Drosophila* PMM2 shows 100% conservation of these 12 active sites (Fig. 1A, red) and identifies numerous additional regions of high 90-100% conservation (Fig. 1A, green). Overall, *Drosophila* PMM2 displays 56% amino acid identity compared to human PMM2 (Fig. 1A). To characterize PMM2 requirements, we first made null mutants using CRISPR/Cas9 genome editing directed at both 5' and 3' ends of *Drosophila pmm2* (Fig. 1A; Gratz et al., 2013). A total of 15 mutations were produced, all verified with direct sequencing: 8 frameshifts, 4 insertions, 2 deletions and 1 missense mutation. Two *pmm2* null frameshift mutations were selected for subsequent behavioral, functional and molecular studies, hereafter referred to as $pmm2^{FS1}$ and $pmm2^{FS2}$.

Two independent UAS-RNAi lines (Bloomington *Drosophila* Stock Center #42956 and Vienna *Drosophila* Resource Center v107619) were used to differentially reduce *pmm2* levels. Quantitative PCR (qRT-PCR) with ubiquitous (UH1-Gal4) expression shows both RNAi lines knockdown *pmm2* transcripts by >77%, a significant ($p<0.001$) reduction compared to UH1-Gal4/+ transgenic controls. Of the two lines, 42956 is significantly more effective than 107619 in reducing *pmm2* levels ($UH1>RNAi^{107619}$, 1.57±0.10; $UH1>RNAi^{42956}$, 1.27±0.10; n=15, p=0.016) compared to control (UH1-Gal4/+, 7.00±0.79, n=15). Moreover, at 50% lethality of ubiquitous *pmm2* knockdown (42956) (Fig. 1B), *pmm2* levels in UH1-Gal4/+ controls show a sharp increase (1^{st} instar, 1.40±0.15, n=8; 2^{nd} instar

7.00±0.79, n=15), which is paralleled by the surviving ubiquitous *pmm2* knockdown (107619), permitting higher levels of maintained *pmm2* expression. The strong (42956) and weak (107619) PMM2 knockdown phenotypes are likely the result of the significant differences in transcript levels.

Null *pmm2* mutants, heteroallelic combinations and mutants over deficiency all show identical early larval lethality during the late 1st to early 2nd instar transition (Fig. 1B). Half-time survival (HTS) is similar (e.g. $pmm2^{FS1}$ HTS 51 hours post-hatching (hph), n=73; $pmm2^{FS1}$/Df HTS 46 hours post-hatching (hph), n=79; $pmm2^{FS2}$/Df HTS 51 hours post-hatching (hph), n=84; $pmm2^{FS1}/pmm2^{FS2}$ HTS 52 hph, n=75). Ubiquitous *pmm2* knockdown (42956) results in lifespan only marginally longer than *pmm2* nulls (HTS: 68 hph; n=63), whereas the weaker ubiquitous *pmm2* knockdown (107619)allows survival to late larval stages (HTS: 168 hph; n=90) with some pupation (mean 192 hph; Fig. 1B). UH1/+ controls pupate at 96 hph, showing ubiquitous *pmm2* knockdown (107619)exhibits severe developmental delay. Muscle-specific 24B-Gal4 with the stronger $RNAi^{42956}$ produces 100% pupal lethality, whereas weaker 24B>$RNAi^{107619}$ survives with reduced adult lifespan (HTS: 10 days; n=159) compared to control (24B-Gal4/+, HTS: 38 days; n=79; Fig. 1B). Targeted neural *elav*-Gal4 with $RNAi^{42956}$ exhibits similarly reduced adult lifespan (HTS: 17 days; n=92), which is conversely extended with weak *elav*>$RNAi^{107619}$ (HTS: 65 days; n=51) compared to control (*elav*-Gal4/+, HTS: 39 days; n=68; Fig. 1B). This suggests a delicate PMM2 balance, with strong neural loss detrimental but moderate neural loss extending lifespan. Due to these lethality constraints, hereafter weaker $RNAi^{107619}$ is used for ubiquitous knockdown and stronger $RNAi^{42956}$ is used for tissue-targeted neural and muscle knockdown.

Neuronal PMM2 maintains normal posture and coordinated movement

Neurological movement symptoms in CDG-Ia patients range from slight gait ataxia to severe cerebellar ataxia; most children are unable to walk unassisted, and most adults are wheel-chair bound (Barone et al., 2014; Barone et al., 2015; Marquardt and Denecke, 2003; Monin et al., 2014). Loss of *Drosophila* PMM2 results in similarly severe postural and movement phenotypes, largely due to nervous system involvement. Targeted neural *elav*-Gal4 knockdown results in a highly penetrant "held-out wings" posture (Fig. 1C), which is associated with defects in flight muscle control of wing positioning (Muller et al., 2010; Zaffran et al., 1997). Neural *pmm2* knockdown adults have severe ataxia, with profound incoordination, inability to walk in a directed fashion and complete inability to fly. Weak muscle-specific PMM2 knockdown does not yield ataxia. However, strong muscle-specific knockdown allows pupae to develop fully, but not a single pharate adult properly ecloses. A few animals partially eclose before dying, and animals mechanically freed from pupal cases do not move or survive. Based on these severe qualitative movement defects, we conducted a range of quantitative analyses (Fig. 1D).

Larval locomotion requires a CNS pattern generator driving coordinated stimulation of segmental nerves to drive neuromuscular junction (NMJ) transmission evoking coordinated muscle contraction (Gjorgjieva et al., 2013; Kohsaka et al., 2014; Nichols et al., 2012; Sokolowski, 1980). Locomotion was assayed on apple juice agar plates, monitoring movement from the barren center to a yeast reward located along the rim (Fig. 1D, left). At 24 hph, *pmm2* null 1st instar mutants display a significant reduction in coordinated movement, as measured in peristaltic waves/second ($pmm2^{FS2}$, 0.71±0.06 w/s; n=17) compared to genetic control (w^{1118}, 1.04±0.02 w/s; n=17; p<0.0001; Fig. 1E). Both lifespan and movement data show ubiquitous *pmm2* knockdown (42956) phenocopies the *pmm2*

genetic nulls. Similarly, 3rd instar ubiquitous *pmm2* knockdown (107619)show a comparable reduction in larval locomotion in peristaltic waves/second (0.51±0.04 w/s; n=20) compared to controls (UH1-Gal4/+, 1.06±0.04 w/s; n=20, p<0.0001; Fig. 1E). Thus, global PMM2 loss dramatically impairs coordinated movement needed to maintain viability.

Neural-specific PMM2 involvement was next tested in adults, using a range of established assays (Nichols et al., 2012). Negative geotaxis assays animals the ability to climb vertically (2cm) from the bottom of a vial (Fig. 1D, middle). Neurally-targeted *elav*-Gal4>RNAi^{42956} prevents this simple task, whereas nearly all control animals display the necessary coordinated locomotion at 5 seconds (*elav*-Gal4/+, 90±2.1%, n=50) and 10 seconds (*elav*-Gal4/+, 93±2.4%, n=50; Fig. 1F). Not a single *pmm2* RNAi animal performed the task (n=40, p<0.0001). A less demanding horizontal locomotion assay measures the time required to escape a 4cm diameter circle (Fig. 1D, right). Neurally-targeted *elav*-Gal4>RNAi^{42956} results in a 150-fold delay (302.0±60.02 sec; n=15) compared to controls (*elav*-Gal4/+, 1.93±0.32 sec; n=15; p<0.0001; Fig. 1G). Mutants exit the ring by uncoordinated flailing/kicking, with only a few animals crossing the circle in a directed, purposeful manner. These results show a strong PMM2 role for coordinated movement, similar to CDG-Ia patient symptoms, with a striking PMM2 impact on neurons.

PMM2 loss suppresses N-glycosylation and enhances glycan turnover

To assess N-linked glycoprotein glycosylation levels correlating with movement defects in *pmm2* null mutants and neurally-targeted RNAi knockdown, we next assayed glycome composition. Human CDG-Ia patients display altered glycosylation status, including reduced concanavalin A (ConA) binding but increased fucose-decorated glycoproteins (Dijk et al., 2001). In *Drosophila*, at all stages of development and in all tissues, the major N-linked glycoprotein constituent glycans include high-mannose and pauci-mannose (≥3

mannose residues) classes, whereas human glycosylation is typically more branched and complexly decorated (ten Hagen et al., 2009; Katoh and Tiemeyer, 2013). Complex hybrid and branched N-glycans are present in *Drosophila*, but at much lower relative abundances (Aoki et al., 2007). Here, *Drosophila* N-linked glycans were analyzed by mass spectrometry (MS) throughout the larval body in *pmm2* null mutants and with combined neuronal (*elav*-Gal4) and muscle (24B-Gal4) *pmm2* RNAi, and in adult heads only with neurally targeted *pmm2* RNAi (Fig. 2).

N-linked glycans were released from equal amounts of input *pmm2* null ($pmm2^{FS1}$) compared to genetic background control (w^{1118}). Proteins analyzed by MS were dramatically reduced for all major classes (high-mannose, pauci-mannose and complex; Fig. 2A). For example, the relative abundance of $Man_9GlcNAc_2$ (m/z=1210.1, doubly-charged), a dominant structure in the glycan profile, is down 4-fold in *pmm2* null mutants (Fig. 2A; dashed line). All other detected N-glycans exhibit comparable reductions, consistent with a global suppression of glycoprotein glycosylation. A similar global reduction occurs in 3rd instar larva using paired neural and muscle Gal4s to drive *pmm2* RNAi (*elav*,24B>$RNAi^{42956}$; Fig. 2B). Interestingly, neurally-targeted *pmm2* RNAi in the adult head does not produce the same phenotype. N-linked glycan quantities are relatively comparable for transgenic control (*elav*-Gal4/+) and this targeted *pmm2* knockdown (*elav*-Gal4>$RNAi^{42956}$; Figs. 2C). Major complex N-linked glycans (e.g. NM_3N_2F, m/z=1591.0, singly-charged) are not noticeably changed in abundance. However, pauci-mannose glycans display clearly increased abundance. For example, the core-fucosylated trimannosyl glycan M_3N_2F (m/z=1345.7, singly-charged) is increased in relative abundance, as is non-fucosylated M_3N_2 (m/z=1172.0, singly charged), with *pmm2* knockdown (Figs. 2C).

Loss of N-linked glycoprotein glycosylation in $pmm2^{FS1}$ mutants implies decreased efficiency in glycosylation initiation by the oligosaccharyltransferase complex (OST) in the

endoplasmic reticulum, and/or increased ERAD-mediated protein deglycosylation within the cytoplasm (Gao et al., 2011). Either mechanism should be reflected in increased abundance of free oligosaccharide (FOS), branched oligosaccharides unbound to lipid or protein,, either due to endogenous PNGase release or via lipid-linked precursor hydrolysis by the OST (Cline et al., 2011; Gao et al., 2011). Consistently, FOS abundance is strikingly increased in *pmm2*^{FS1} mutants (Fig. 3A). FOS abundance is detected as products of PNGase and endo-N-acetylglucosaminidase digestion (N1, blue asterisks) or glycans possessing two reducing terminal GlcNAc residues (N2, red asterisks; Fig. 3A), with total ion mapping chromatograms filtered for loss of non-reducing terminal HexNAc residues. Both FOS classes are increased in *pmm2* nulls compared to control (Fig. 3A). Thus, glycomics and FOS assays show striking reduction in mature glycan abundance globally, and altered glycomic repertoire in the nervous system with PMM2 loss. To test for cellular requirements, we next moved to the well-characterized NMJ driving movement.

PMM2 maintains the normal glycan environment in the NMJ synaptomatrix

Glycan-binding lectin probes have long been used to chart the cellular carbohydrate landscape at both mammalian and *Drosophila* synapses (Jumbo-Lucioni et al., 2014; Parkinson et al., 2013; Schneider et al., 2011). To assay the composition of the heavily-glycosylated larval NMJ synaptomatrix, we utilized a panel of lectins, including *Erythrina cristagalli* (ECL) to label D-galactose glycans, *Vicia villosa* (VVA) to label N-acetylgalactosamine glycans, and anti- horseradish peroxidase (HRP) to lab alpha1-3-linked fucose moieties (Jumbo-Lucioni et al., 2014; Kurosaka et al., 1991). Both ECL and VVA reveal strong reductions in ubiquitous *pmm2* knockdown (107619) compared to the UH1-Gal4/+ controls (Fig. 3B). Quantification reveals >50% ECL reduction (UH1-Gal4>RNAi^{107619}, 0.43±0.05; UH1-Gal4/+, 1.00±0.08; n=24; $p<0.0001$) and >30% VVA

reduction (UH1-Gal4>RNAi^{107619}, 0.69±0.05; UH1-Gal4/+, 1.00±0.05; n=24; p<0.0001; Fig. 3C). HRP is reduced by ≥20% (UH1-Gal4>RNAi^{107619}, 0.79±0.06; UH1-Gal4/+, 1.00±0.06; n=24; p≤0.01; Fig. 3C). Dual neural and muscle knockdown *elav*-Gal4,24B-Gal4 RNAi also exhibits ≥20% HRP loss (*elav*-Gal4,24B>RNAi^{42956}, 0.79±0.06; *elav*-Gal4,24B/+, 1.0±0.04; n≥26, p<0.008). These results indicate a robustly altered glycan composition within the NMJ synaptomatrix, which earlier studies have linked to defects in NMJ structural and functional development.

PMM2 restricts NMJ structural growth and synaptic bouton differentiation

Loss of synaptomatrix glycosylation has been shown to result in elevated structural elaboration of the *Drosophila* NMJ, as evidenced by increased branching and excess synaptic boutons (Jumbo-Lucioni et al., 2014; Parkinson et al., 2013). To examine NMJ architecture, we characterized wandering 3rd instar muscle 4 NMJs labeled for HRP and Discs Large (DLG), to illuminate pre- and postsynaptic compartments, respectively (Fig. 4A). Synaptic branches (defined as HRP-positive processes with >2 boutons), boutons (defined as DLG-positive synaptic varicosities >1μm in diameter) and NMJ terminal area (based on DLG-positive labeling) were all quantified (Fig. 4B-D). Cell-specific requirements were tested with neuronal (*elav*) and muscle (24B) targeted Gal4 drivers in comparison to ubiquitous (UH1-Gal4) *pmm2* knockdown. In all cases, loss of PMM2 results in clear NMJ overelaboration, with more branches and supernumerary type Is/Ib synaptic boutons, with ubiquitous RNAi resulting in the greatest level of unrestrained NMJ overgrowth (Fig. 4).

PMM2 loss increases NMJ branching, due to both pre- and postsynaptic roles (Fig. 4A). Ubiquitous *pmm2* RNAi increases branch number ~2-fold (UH1-Gal4>RNAi^{107619}, 6.3±0.36 branches, n=24) compared to controls (w^{1118}, 3.7±0.19, n=88; UH1-Gal4/+, 3.9±0.38 branches, n=22; p<0.0001; Fig. 4B). Likewise, neural (*elav*) and muscle (24B)

knockdown more weakly increase terminal branch number (*elav*, 5.7±0.40; 24B, 4.2±0.39; *elav,*24B, 5.7±0.33 branches) compared to transgenic controls (*elav-Gal4*/+, 4.0±0.47; 24B-Gal4/+, 3.0±0.24; *elav,*24B-Gal4/+, 3.5±0.37 branches; $p<0.01$, $p<0.01$ and $p<0.0001$ respectively; Fig. 4B). Consistently, bouton number is elevated >2-fold with ubiquitous PMM2 removal (UH1-Gal4>RNAi^{107619}, 88±3.9 boutons, n=24) relative to controls (w^{1118}, 32±1.4, n=88; UH1-Gal4/+, 36±2.4 boutons, n=22; $p<0.0001$; Fig. 4C). Bouton number is also elevated with neural and muscle knockdown (*elav*, 61±3.8; 24B, 42±3.0; *elav*,24B, 56.5±2.9 boutons) compared to controls (*elav-Gal4*/+, 39±3.3; 24B-Gal4/+, 30±2.0; *elav*,24B/+, 31.8±2.7 boutons; $p<0.0001$, $p<0.001$ and $p<0.0001$ respectively; Fig. 4C). Finally, analyses of synaptic terminal area show increased size with ubiquitous, neuronal and co-neural/muscle PMM2 loss ($p<0.01$, $p<0.0001$ and $p<0.0001$, respectively), but with no significant change upon muscle-specific PMM2 removal (Fig. 4D).

Synaptic over-elaboration defects occur across the neuromusculature. Compared to the above lateral muscle 4 defects (Fig. 4), ventral muscles 6/7 exhibit comparable NMJ phenotypes. For example, the synaptic area in *elav*-Gal4,24B-Gal4/+ transgenic controls (380.82μm^2) is dramatically expanded in neural and muscle combined knockdown *elav*-Gal4,24B-Gal4<RNAi^{42956} (526.82μm^2), a highly significant ($p>0.0001$) increase. Early lethal *pmm2* genetic null mutants also exhibit similarly increased NMJ growth and structural elaboration in the 1st instar prior to developmental arrest (Fig. 5). Using the structural parameters as above, *pmm2* nulls manifest increased synaptic branch number (w^{1118}, 1.6±0.11; *pmm2*^{FS2}, 2.2±0.14 branches; $p=0.007$; Fig. 5B), more bouton formation (w^{1118}, 5.6±0.21; *pmm2*^{FS2}, 7.0±0.32 boutons; $p=0.0006$; Fig. 5C) and dramatically increased synaptic area (w^{1118}, 1.0±0.07; *pmm2*^{FS2}, 1.5±0.05 ; $p=0.0001$; Fig. 5D). Consistently, *pmm2* null mutants exhibit a loss of synaptic N-linked glycosylation, including ≥20% decrease in HRP glycan labeling (w^{1118}, 1.0±0.08; *pmm2*^{FS2}, 0.80±0.04; $n\geq30$, $p\leq0.05$; Fig. 5E). To

determine how NMJ overgrowth compares to synaptic function, we next turned to electrophysiological studies.

Coupled pre- and postsynaptic PMM2 function limits NMJ transmission strength

Glycosylation has been shown to play key roles in NMJ functional differentiation and the determination of neurotransmission strength (Dani et al., 2012; Dani et al., 2014; Parkinson et al., 2013). The severely impaired coordinated locomotion and alterations in NMJ structure similarly suggest PMM2 roles in synaptic function. We tested neurotransmission in the two-electrode voltage-clamp (TEVC) recording configuration, by stimulating the motor nerve with a glass suction electrode and measuring the evoked excitatory junctional current (EJC) from the voltage-clamped muscle (Parkinson et al., 2013). To compare EJC transmission properties, 10 consecutive stimulation recordings were made at 0.2Hz, and then averaged to calculate the mean peak transmission amplitude. Cell-specific roles in functional differentiation were tested with targeted neuronal (*elav*) and muscle (24B) Gal4 drivers, alone and in combination, in comparison to ubiquitous (UH1-Gal4) *pmm2* RNAi knockdown (Fig. 6).

PMM2 loss dramatically increases neurotransmission strength due to an unusual coupled role in both pre- and postsynaptic cells (Fig. 6A). Sample recordings show that all transgenic controls and the genetic background control (w^{1118}) have comparable EJC properties, and only ubiquitous and combined pre- and postsynaptic PMM2 knockdown strongly and equally increase transmission amplitude (Fig. 6A). Ubiquitous RNAi increases peak EJC values by ~75% (UH1-Gal4>RNAi^{107619}, 1.73±0.09 (450.2±23.72nA), n=21; w^{1118}, 1.00±0.03 (253.68±8.26nA), n=44; UH1-Gal4/+, 1.11±0.06 (288.57±14.39nA), n=21; $p<0.0001$; Fig. 6B). Strong PMM2 knockdown in either neuron (*elav*-Gal4>RNAi^{42956}, 1.03±0.04 (301.8±12.66nA), n=16) or muscle (24B-Gal4>RNAi^{42956}, 1.20±0.05

(320.7±13.41nA), n=18) has no significant impact on amplitude compared to controls (*elav*-Gal4/+, 0.99±0.04 (289.9±12.09nA), n=17; 24B-Gal4/+, 1.20±0.04 (302.4±10.90nA), n=16; Fig. 6B). However, coincident *pmm2* RNAi driven in both the presynaptic neuron and postsynaptic muscle again shows significantly ($p<0.0001$) increased EJCs (*elav*-Gal4,24B-Gal4>RNAi^{42956}, 1.91±0.05 (397.61±11.58nA), n=23) compared to the dual driver control alone (*elav*-Gal4,24B-Gal4/+, 1.11±0.07 (231.0±14.56nA), n=23; Fig. 6B). We next recorded miniature evoked junction currents (mEJC) in neural and muscle combined knockdown *elav*-Gal4,24B-Gal4>RNAi^{42956} but did not detect any significant change in either frequency (*elav*-Gal4,24B-Gal4/+, 1.80±0.11 Hz; *elav*-Gal4,24B-Gal4/42956, 1.93±0.14 Hz; n.s. n=20) or amplitude (*elav*-Gal4,24B-Gal4/+, 0.66±0.02 nA; *elav*-Gal4,24B-Gal4/42956, 0.61±0.03 nA; n.s. n=20) compared with control but quantal content (QC) was elevated >80% (*elav*-Gal4,24B-Gal4/+, 362.0±13.9 QC; *elav*-Gal4,24B-Gal4/42956, 677.6±29.9 QC; Fig. 6C)). Thus, PMM2 specifically regulates evoked quantal content (Fig. 6C). These results indicate the NMJ functional defect is not cell autonomous, as either pre- or postsynaptic PMM2 is sufficient to properly regulate neurotransmission strength. We therefore began to test non-cell autonomous molecular mechanisms that could underlie the PMM2 function.

PMM2 positively regulates the synaptic extracellular matrix proteinase pathway

Extracellular mechanisms in the highly-glycosylated NMJ synaptomatrix provide an obvious answer to PMM2 non-cell autonomous phenotype. We were first guided to consider extracellular matrix metalloproteinase (MMP) pathways owing to common tracheal break and melanization mutant phenotypes (Glasheen et al., 2010; Page-McCaw et al., 2007; Zhang and Ward, 2009) shared with PMM2 loss-of-function (data not shown). Subsequently, recent work has shown that *mmp* mutants exhibit both NMJ structural and functional phenotypes strikingly similar to PMM2 loss-of-function (Dear et al., 2016). Therefore, we examined the

matrix metalloproteome at the NMJ, which includes secreted MMP1, GPI-anchored MMP2 and their shared secreted tissue inhibitor of MMP (TIMP) (Dear et al., 2016; Kessenbrock et al., 2010; Page-McCaw et al., 2007). We hypothesized that PMM2-dependent glycan modification of these extracellular proteins, and/or their synaptic substrates, could provide a mechanism regulating NMJ structure and function.

Consistent with this hypothesis, utilizing PNGaseF and EndoH to remove N-linked glycosylation (Song et al., 2011) reveals a clear reduction in MMP size (Fig. 7A), showing a high level of glycosylation (Glasheen et al., 2009; Jia et al., 2014). This change is much greater for membrane-anchored MMP2, in which all major isoforms show glycosylation-dependent shifts in size (Fig. 7A, asterisks), compared to secreted MMP1, in which only one minor isoform displays glycosylation. We next tested for non-glycosylated MMP forms in mutants using UH1-Gal4 driven *pmm2* knockdown (Fig. 7A). Loss of PMM2 results in multiple shifted (non-glycosylated) MMP bands compared to controls. Again, the effect is much greater for MMP2, with multiple bands showing a PMM2-dependent loss of glycosylation (Fig. 7A, asterisks). Consistently, NMJ labeling in *pmm2* RNAi compared to controls shows the synaptic matrix metalloproteome is compromised, again particularly for MMP2 (Fig. 7B). PMM2 ubiquitous knockdown results in >50% reduction in MMP2 levels (UH1-Gal4>RNAi^{107619}, 0.44±0.04, n=32) normalized to control (UH1-Gal4/+, 1.00±0.08, n=32; $p<0.0001$; Fig. 7C). In contrast, there is no significant change in MMP1 expression, although there is a slight decreasing trend (UH1-Gal4>RNAi^{107619}, 0.87± 0.07, n=20; UH1-Gal4/+, 1.00±0.07, n=24; Fig. 7B.C). TIMP is also reduced with PMM2 loss (UH1-Gal4>RNAi^{107619}, 0.60±0.07, n=24) compared to control (UH1-Gal4/+, 1.00±0.08, n=24; $p<0.001$; Fig. 7B,C). These results show synaptic MMP2 is strongly reduced by PMM2 removal, with a reduction also in synaptic TIMP levels. Given the importance of the synaptic

metalloproteome in shaping Wnt *trans*-synaptic signaling (Dear et al., 2016), we next tested predicted PMM2 involvement.

PMM2 positively regulates the Wnt Wingless *trans*-synaptic signaling pathway

MMPs play an important role in Wnt Wingless (Wg) intercellular signaling by directly regulating the HSPG Dally-like protein (Dlp) Wg co-receptor (Wang and Page-McCaw, 2014). Importantly, the same Wg/Dlp signaling pathway is a critical driver of structural and functional development at the *Drosophila* NMJ (Ataman et al., 2006, 2008; Kerr et al., 2014; Mathew et al., 2005) and is known to be modulated by glycan mechanisms (Dani et al., 2012; Jumbo-Lucioni et al., 2014; Parkinson et al., 2013). Wg binds the Frizzled-2 (Fz2) receptor, which is internalized and the C-terminus proteolytically cleaved (Fz2C) for transport via the Fz2C nuclear import (FNI) pathway (Ataman et al., 2006; Mathew et al., 2005) to modulate NMJ structure/function (Speese et al. 2012). Based on this extensive work, we hypothesized that PMM2 regulates MMP2-dependent Wg signaling to regulate NMJ structure and function underlying coordinated movement and maintained viability.

All 3 components of the signaling pathway show clear down-regulation with PMM2 loss (Fig. 8). Qualitative comparison of Wg ligand and Dlp co-receptor at the NMJ, and Fz2C cleavage/import into the postsynaptic muscle nuclei, all show reduction of pathway components and impairment of downstream signaling (Fig. 8A). Quantification of the extracellular Wg levels shows a ~50% reduction with PMM2 ubiquitous knockdown (UH1-Gal4>RNAi^{107619}, 0.55±0.05, n=32) normalized to control (UH1-Gal4/+ 1.00±0.11, n=30; $p<0.001$; Fig. 8B, left). Wg co-receptor Dlp is also reduced (UH1-Gal4>RNAi^{107619}, 0.72±0.07, n=24) compared to control (UH1-Gal4/+, 1.00± 0.06, n=24, $p<0.01$; Fig. 8B, middle). Finally, consequent Fz2C import into the muscle nucleus via the FNI pathway to mediate downstream signaling is significantly impaired with PMM2 ubiquitous knockdown

(UH1-Gal4>RNAi^{107619}, 0.78±0.05, n=24) compared to control (UH1-Gal4/+, 1.00±0.04, n=24), showing a significant decrease in *trans*-synaptic signaling ($p<0.01$; Fig 8B). These results agree well with the recent report of strongly reduced Wnt signaling in the *Xenopus* PMM2-CDG model (Himmelreich et al., 2015). We conclude that neurological impairments in the *Drosophila* PMM2-CDG model similarly map to impaired Wnt signaling, to misregulate NMJ synaptogenesis underlying coordinated movement.

Discussion

We set forth to establish a *Drosophila* CDG-Ia (aka PMM2-CDG) genetic model through manipulation of the causative phosphomannomutase type 2 (PMM2) gene (Freeze et al., 2014). Using CRISPR-generated *pmm2* null mutants and transgenic RNAi, we found PMM2 levels correlated to coordinated movement abilities and lifespan (Fig. 1), as in CDG-Ia patients (Cylwik et al., 2013; Jaeken, 2013; Lonlay et al., 2001). Human patients with identical *pmm2* mutations present with a wide spectrum of movement defects (Marquardt and Denecke, 2003; Schneider et al., 2011), attributed to genetic and/or environmental factors readily controlled in *Drosophila*. With tissue-specific drivers, we found a neural PMM2 impairment for coordinated movement (Fig. 1). Interestingly, weak neural knockdown of *pmm2* resulted in increased lifespan. Similarly, moderate impairments of oxidative stress and dietary restriction pathways have also been reported to extend lifespan (Mair et al., 2005; Min and Tartar, 2006; Ristow and Schmeiser, 2011). Like PMM2, severe impairments of these pathways result in reduced lifespan and early death, but more modest impairments extend lifespan via changes in metabolic rate, developmental conditioning and/or defense mechanisms. Null *pmm2* mutants display severe attenuation of glycoprotein glycosylation (Fig. 2), with reduced N-linked glycosylation diversity (Aoki et al., 2007). Similar global N-glycan losses occur with strong *pmm2* RNAi throughout the larval neuromusculature, but not with weaker neural-targeted *pmm2* RNAi in the adult head (Fig. 2). Lipid-linked oligosaccharides (LLO) used for protein attachment by oligosaccharyltransferase (OST) activity are regulated at many levels (Gao et al., 2011). PMM2 loss should reduce LLO levels by inhibiting mannose-1-phosphate production and elevating the mannose-6-phosphate pool acting as a signal mediating LLO destruction, thereby increasing free oligosaccharides (FOS; Fig. 3A; Gao et al., 2011). However, the increase in pauci-mannose structures with adult neuronal *pmm2* knockdown differentially alters glycan maturation. The mannose-6-phosphate

increase may change the mannose phosphoisomerase (MPI) equilibrium, leading to interconversion of mannose-6-phosphate to fructose-6-phosphate to siphon LLO-toxic mannose-6-phosphate and mitigate LLO elimination.

Null *pmm2* mutants display elevated FOS levels (Fig. 3A). Increased phosphorylated FOS levels, predicted to be cleaved from LLO intermediates, likewise occur in CDG-Ia patient cells (Vleugels et al., 2011). Similarly, the zebrafish morpholino model shows increased FOS levels, with phenotype rescue via MPI co-reduction, suggesting causative mannose-6-phosphate elevation (Cline et al., 2012). Viable human CDG-Ia patients are typically heterozygous for *pmm2* mutations, resulting in partial loss of PMM2 (Matthijs et al., 1998; Monin et al., 2014). In *Drosophila*, partial loss-of-function from neuron-targeted RNAi results in surprising resistance to glycosylation changes (Fig. 2C). Pauci-mannose glycans are increased, but high mannose and complex glycans unchanged. PMM2 regulates GDP-mannose availability for glycan production, but following glycosylation by OST further processing should be GDP-mannose independent (Cylwik et al., 2013). The increased pauci-mannose glycans resulting from PMM2 partial loss suggests GDP-mannose levels influence glycan processing beyond the role as synthetic donors for mannosylation. Pauci-mannose glycan production is driven by the balance between Golgi exomannosidases, GlcNAc-Transferase 1 and a hexosaminidase removing GlcNAc from nascent complex glycans (Stanley et al., 2009). Precursor abundances, including donor and acceptor, influence expression and activity of glycan-processing enzymes. Reduced GDP-mannose likely skews the balance of enzyme activities that trim high-mannose to pauci-mannose, before they increase in complexity. Impacts on glycosylation independent of GDP-mannose is also evident in reduced NMJ lectin labeling with PMM2 loss (Fig. 3B). Importantly, both ECL and VVA bind mannose-free structures, most likely on O-linked glycoprotein backbones.

The nervous system is tightly regulated by glycans at multiple levels of development and function (Koles et al., 2007; Scott and Panin, 2014a,b; Seppo and Tiemeyer, 2000). NMJ architectural overelaboration and functional strengthening has been identified in many glycan mutants in our systematic genetic screens, including *sulf1*, *mgat1*, *galt* and *pgant* (Dani et al., 2012; Dani et al., 2014; Jumbo-Lucioni, 2014; Parkinson et al, 2013). Consistently, PMM2 loss shows striking NMJ overelaboration (Fig. 4), supporting the conclusion that glycans primarily inhibit synaptic morphogenesis. Null *pmm2* mutants already exhibit strong synaptic architecture defects within a day after hatching (Fig. 5), showing that PMM2-dependent glycan mechanisms brake the earliest stages of synaptic growth and differentiation. Glycosylation mechanisms also have key roles modulating neurotransmission (Koles et al., 2007; Scott and Panin, 2014a,b), and PMM2 loss strongly increases NMJ function (Fig. 6). There is no effect on spontaneous synaptic vesicle release or postsynaptic amplitude, indicating a specific PMM2 role in limiting stimulus evoked quantal content. Interestingly, neural- and muscle-targeted PMM2 knockdown have no effect on transmission, however combined neural and muscle knockdown fully replicates the ubiquitous PMM2 loss phenotype (Fig. 6), indicating that the elevated transmission needs concomitant PMM2 removal both pre- and postsynaptically. One explanation is that semi-synaptic glycosylation may be sufficient to normalize transmission: loss of glycosylation from one side may be compensated for by the other side, as synapse transmission is highly regulated by both pre- and postsynaptic cells (Dani and Broadie, 2012). Another idea is that glycosylation could be provided by extracellular components from either synaptic partner cell.

The non-cell-autonomous defect occurring with PMM2 loss prompted us to investigate extracellular signaling mechanisms, which are tightly regulated by glycosylation at the NMJ (Dani et al. 2012; Dani et al., 2014; Parkinson et al., 2013; Jumbo-Lucioni et al., 2014; Rushton et al., 2012). In particular, matrix metalloproteinases (MMPs) play critical

roles shaping synapse structure and function (Dear et al., 2016; Kessenbrock et al., 2010; Page-McCaw et al., 2007; Sternlicht and Werb, 2001). PMM2 loss could impair MMP glycosylation or ability to cleave improperly glycosylated substrates (Godenschwege et al., 2000; Llano et al., 2000; Llano et al., 2002; Pohar et al., 1999). PNGaseF and EndoH treatment to remove N-linked glycans shows MMP2 isoforms are highly glycosylated, whereas only a tiny subset of MMP1 isoforms are glycosylated (Fig. 7A). GPI-anchored MMP2 also requires GDP-mannose, although GPI anchors require fewer donor mannose than N-linked glycans (Morena-Bario et al., 2013). Importantly, *pmm2* RNAi similarly removes glycosylation from multiple MMP2 isoforms, with only a minor change to MMP1 (Fig. 7A). As predicted by PMM2-dependent glycosylation changes, MMP2 is strongly reduced at the NMJ synapse with *pmm2* RNAi, whereas MMP1 is not significantly altered (Fig. 7B,C). The TIMP regulator is also reduced in abundance with removal of PMM2, which would be predicted to help alleviate consequences of MMP2 loss, perhaps as a compensation mechanism (Dear et al., 2016). Importantly, recent work from our lab has shown that MMPs play critical roles regulating NMJ structural and functional synaptogenesis via control of heparan sulfate proteoglycan (HSPG) receptors that modulate Wnt *trans*-synaptic signaling (Dear et al., 2016).

Recent work utilizing PMM2 morpholino knockdown in *Xenopus* revealed altered glycosylation of Wingless-type MMTV integration site family growth factor (Wnt) and reduction of Wnt signaling (Himmelreich et al., 2015). Similarly, we find that *pmm2* RNAi knockdown in *Drosophila* suppressing Wnt Wingless (Wg) signaling at the developing NMJ synapse (Fig. 8). With PMM2 loss, synaptic levels of Wg ligand and its HSPG co-receptor Dally-like Protein (Dlp) are both strongly reduced, and downstream signaling through the Frizzled Nuclear Import (FNI; Speese et al., 2012) pathway is consistently down-regulated (Fig. 8). These defects have been previously associated with the loss of synaptic MMP2,

which acts via Dlp to regulate Wg *trans*-synaptic signaling to modulate both structural and functional NMJ development in the same direction (Dear et al., 2016). However, we have shown that PMM2 loss has myriad consequences on N-linked glycoprotein glycosylation, and therefore quite likely impacts NMJ synaptogenesis at multiple levels. Indeed, specifically targeted reduction in Wg signaling alone has previously been associated with decreased NMJ structural development and reduced function (Ataman et al., 2008; Kerr et al., 2014; Packard et al., 2002), which differs from the Wg attenuation associated with PMM2 loss. Therefore, PMM2 roles at the NMJ synapse likely reflect roles in multiple intersecting pathways that jointly control growth, structural differentiation and neurotransmission strength. Our future work will aim at deciphering other PMM2-dependent glycoprotein contributions, which combinatorially result in the structural and functional NMJ defects characterizing this CDG-Ia disease state model.

We hope this new *Drosophila* model will prove instrumental for tackling the disease, and related CDGs, especially in regard to neurological symptoms (Grunewald, 2009; Jaeken, 2010). One avenue will be to dissect roles played by glycan precursors and mannose-6-phosphate buildup, by examining genetic interactions shifting the relative abundance of alternatively processed glycans and to alleviate increased FOS levels. For example, using genetic MPI reduction or pharmaceutical MPI inhibitors in the benzoisothiazolone series (Sharma et al., 2011). One such agent, MLS0315771, has been shown to favor mannose-1-phosphate production in CDG-Ia patient fibroblasts and zebrafish embryos. Pharmacological tests in *Drosophila* could include assays to prolong lifespan, improve coordinated movement and prevent NMJ structural and functional defects. The current standard of care for CDG-Ia patients is simply symptomatic treatment and disease management (Grunewald, 2009; Jaeken, 2013). The mouse model suggests beneficial dietary intervention, common for other metabolic disorders like Classic Galactosemia (Jumbo-Lucioni et al., 2014). However,

mannose treatment has not been effective in restoring N-linked glycoprotein glycosylation levels in CDG-Ia patients (Thiel and Korner, 2013). Drug avenues to increase PMM2-dependent glycosylation are hypothesized, but there are no studies (Thiel and Korner, 2013). We expect the relatively high speed of *Drosophila* disease model studies utilizing the powerful *Drosophila* genetic toolkit will open up new avenues for disease intervention. We propose here that targeting the matrix metalloproteome and Wnt signaling pathways offers potential new candidates to consider in developing future CDG-Ia treatments.

Materials and Methods

Drosophila Genetics

Drosophila stocks were grown on standard cornmeal/agar/molasses food in a 12 hour light:dark cycle at 25°C. Mutants were generated with CRISPR/Cas9 (Gratz et al., 2013). Briefly, chiRNA targeting 5'CATTGAAGCGTGATGAAATC and 3'AGGATACGCAACGATTCTC sequences of *pmm2* were incorporated into a pU6-BbsI-chiRNA plasmid (Addgene #45946). F1 progeny from w^{1118} vas-Cas9 males (BDSC# 51324) crossed to w^{1118} Lig4 females (BDSC# 28877) were injected with both targeting plasmids (BestGene Inc., Chino Hills, CA). Injected animals were then crossed to a double balanced (TM3Sb/TM6Tb) mate. F1 males were then crossed to deficiency/balancer females (w^{1118}; Df(3L)BSC380/TM6C, Sb^1cu^1 (BSCD #24404)) to identify lethal *pmm2* mutations. F1 males were recollected and mated with double balanced females to produce the *pmm2* mutant stocks. Mutant backcrossing and sequencing were performed with standard *Drosophila* genetic and PCR techniques. The w^{1118} background stock was used as the control. RNAi studies were performed with neuronal-specific *elav*-Gal4, muscle-specific 24B-Gal4 and ubiquitous UH1-Gal4 transgenic drivers (Brand and Perrimon, 1993; Lin and Goodman, 1994; Rohrbough et al., 2007). Two *pmm2* UAS-RNAi lines, v107691 (Vienna *Drosophila* RNAi Center) and BDSC42956 (Bloomington *Drosophila* Stock Center) were used, with Gal4 drivers alone as transgenic controls.

PCR Methods

For reverse transcription quantitative PCR (RT-qPCR), total RNA was extracted using a Zymo Research Direct-zol RNA Miniprep Plus Kit with TRI reagent (R2070) with on column DNase treatment. The Superscript VILO cDNA synthesis kit (11754-050) was used for cDNA synthesis. RT-qPCR was run on a Biorad CFX96 with equal amounts of cDNA

(2ng for each trial). For expression quantification, the Pfaffl Method was used with standards of known transcript number to quantify absolute cDNA number for target and reference genes. For the reference, ribosomal protein L32 (CG7939) levels were used for normalization of absolute cDNA quantity ((target/reference)*100). The following primers were used for target and reference: *pmm2* forward AGGCTCGGATCTGGAGAAGA, *pmm2* reverse AATGTCGTACTCGGCGAACA; *L32* forward CGGTTACGGATCGAACAAGC, *L32* reverse CTTGCGCTTCTTGGAGGAGA. Samples and standards were run with gene specific primers in duplicate trials.

Behavioral Assays

Egg lays were collected overnight on apple juice agar plates. Plates were then cleared of larvae, and newly-hatched larvae collected after 1 hour (t=0). Larval lifespan analyses involved daily counts. Adult lifespan analyses required two separate methods. For strong neural *elav*-Gal4>RNAi *pmm2* knockdown and *elav*-Gal4/+ controls, adults were collected at eclosion and maintained in laying pots with filter paper covering apple juice plates with yeast. For all other lifespan assays, adults were maintained in normal fly tubes on cornmeal/agar/molasses food. Adult survival was measured 3 times/week, with animals transferred to fresh plates or tubes. The comparative quantification of survival is reported as the time to which 50% of the animals remain viable (half-time survival, HTS). Adult and larval locomotion were assayed as previously described (Nichols et al., 2012; Sokolowski, 1980). Briefly, larvae were tested on apple juice agar plates with yeast paste spread around edges as an attractant. Individual larvae were placed in the middle of a plate and time-lapse recorded under a dissection microscope with a Cannon Rebel DSLR camera (Melville, NY). Locomotion was assayed as peristaltic waves per second (Gjorgjieva et al., 2013). Adult motility was assayed by negative geotaxis and a ring locomotion assay. For geotaxis, adults

were place in empty fly vials for 15 mins to acclimate, and then tubes were sharply tapped to put animals at the bottom (Nichols et al., 2012). Movement was recorded with a Canon Rebel DSLR camera and the percentage of animals to climb above 2cm measured at timed intervals. To assay horizontal locomotion, a 4cm circle was drawn in a large dish, and flies with amputated wings were placed in the middle of the circle. Movement was recorded with a Canon Rebel DSLR camera and the time required to traverse the circle measured.

Glycomic Analyses

Glycoproteins and free oligosaccharides (FOS) were prepared from staged collections of *pmm2* null 1st instars or *elav*-Gal4>RNAi^{42956} adult heads by homogenization in aqueous/organic solvents and subsequent protein precipitation as described previously (Aoki et al., 2007). Briefly, the aqueous/organic homogenate was centrifuged with glycoproteins recovered in the pellet and FOS from the supernatant (Katoh et al., 2013). Precipitated proteins were washed with cold acetone and dried under a stream of nitrogen to produce samples stored desiccated at -20^{o}C. Protein content was determined by BCA assay of resolubilized material (Pierce). N-linked glycoprotein glycans were prepared from 1 mg aliquots by digestion with trypsin/chymotrypsin, followed by enzymatic release of glycans with PNGaseF (Aoki et al., 2007). FOS were separated by passage over a Sep-pak C_{18} cartridge column (Katoh et al., 2013). N-linked glycans and FOS were permethylated and analyzed by mass spectrometry (MS) using nanospray ionization coupled to linear iontrap and orbital Fourier transform mass analyzers (Discover NSI-LTQ/OrbitrapFT, Thermo-Fisher Scientific). MS spectra were collected over the range m/z=200-2000 and MS/MS fragmentation by collision-induced dissociation (CID; 30-40% normalized collision energy) was acquired over the same m/z range using the total ion mapping function of the XCalibur

instrument software (version 2.0). Annotated glycans were validated by exact mass in full MS and by manual inspection of MS/MS spectra at each of the detected m/z values.

Immunocytochemistry Imaging

Immunocytochemistry studies were performed as described previously (Parkinson et al., 2013). Briefly, all animals were dissected, fixed and labeled identically in the same dish. Wandering 3rd or 1st instars were dissected in physiological saline containing 128mM NaCl, 2mM KCl, 4mM $MgCl_2$, 0.25mM $CaCl_2$, 70mM sucrose, 5mM trehalose and 5mM HEPES (pH 7.1). Preparations were fixed in 4% paraformaldehyde for 10 mins at room temperature (RT) in phosphate buffered saline (PBS). Preparations were then either processed with detergent (PBS + 1% bovine serum albumin (BSA) + 0.2% Triton X-100) for intracellular labeling, or detergent-free (PBS with 1% BSA) for extracellular studies. Primary antibodies included: rabbit anti-horseradish peroxidase (HRP, 1:200; Sigma, St. Louis, MO); conjugated CY2, CY3 or CY5-HRP (1:250, Jackson Labs, West Grove, PA); mouse anti-Wingless (Wg, 1:2; Developmental Studies Hybridoma Bank (DSHB), University of Iowa, Iowa City, Iowa); mouse anti-Discs Large (DLG, 1:200; DSHB). Lectins included: *Vicia villosa* agglutinin (VVA-Tritc, 1:200, E.Y. Laboratories, San Mateo, CA) and *Erythrina cristagalli* lectin (ECL-biotin, 1:250, Vector Labs). Secondary Alexa fluorophore antibodies (Invitrogen, Grand Island, NY) included: goat anti-mouse 488 and 568 (1:250), goat anti-rabbit 488 and 568 (1:250), and streptavidin 488 and 594 (1:250). Primary antibodies and lectins were incubated at 4°C overnight; secondary antibodies were incubated at RT for 2 hours. Samples were mounted in Fluoromount-G (Electron Microscopy Sciences, Hatfield, PA). All preparations were imaged using identical parameters. Z-stacks were taken with a Zeiss LSM510 META laser-scanning confocal using a 63X Plan Apo oil immersion objective. Optical sections were imaged starting above and ending below the NMJ or muscle nuclei to

encompass their entirety. Stacks were projected on the Z-axis for maximum intensity, with NMJ or nuclei signals highlighted and average intensity quantified using ImageJ (Abramoff et al., 2001).

Western Blot analyses

Tissues were homogenized in buffer (1% SDS, 50mM Tris-HCl, 150mM NaCl) with protease inhibitors, heated (70°C, 10 mins) and centrifuged (16,100xg, 10 mins). Supernatant was split into two tubes (+/- enzyme) and glycosidase treatment done following manufacturer instructions (New England Biolabs (NEB), Ipswich, MA). Briefly, samples in denaturing buffer (NEB) were heated (10 mins, at 95°C) then cooled to RT. Denatured samples were treated with or without (buffer alone) Endoglycosidase-H (NEB) and PNGase-F (NEB) at 1 microliter enzyme/ 20 microgram protein in 1X G5 buffer (NEB) overnight at 37°C. Samples were assayed with Western blot SDS-PAGE using 10% Bis-Tris gels and Western blot analysis. Membranes were blocked in 2% milk in tris-buffered saline (TBS) for 1 hour at RT. Mmp antibodies (1:1500) were incubated overnight 4°C, then washed for 5 mins (x6) in TBS + 0.1% Tween-20 (TBST). Goat secondaries (1:10,000; Rockland, Limerick, PA) were incubated for 1 hour RT. Blots washed for 5 mins (x6) in TBS-T were imaged using an Odyssey Infrared Imaging System.

Electrophysiology

Excitatory junctional current (EJC) recordings made using two-electrode voltage-clamp (TEVC) were done as previously reported (Parkinson et al., 2013). Briefly, wandering 3rd instars were glued with 3M Vetbond adhesive (World Precision Instruments, Sarasota, FL) to sylgard-coated glass coverslips, cut longitudinally along the dorsal midline, internal organs removed and sides affixed down for neuromusculature access. Peripheral nerves were cut at

the ventral nerve cord. Recordings were done at 18°C in saline consisting of 128mM NaCl, 2mM KCl, 4mM $MgCl_2$, 1mM $CaCl_2$, 70mM sucrose, 5mM trehalose and 5mM HEPES (pH 7.1), imaged using a Zeiss Axioskop microscope with 40X immersion objective. A fire-polished glass suction electrode was used for evoked nerve stimulation with 0.5 millisecond supratheshold stimuli at 0.2Hz from a Grass S88 stimulator (Rohrbough et al., 2007). Muscle 6 in abdominal segments 2/3 was impaled with two microelectrodes of 10-15 MΩ resistance filled with 3M KCl, and clamped (-60 mV) using an Axoclamp-2B amplifier (Molecular Devices, Sunnyvale, CA). EJC records were filtered at 2kHz. To quantify EJC amplitudes, 10 consecutive traces were averaged. Spontaneous miniature EJC (mEJC) records were made in 2-minute sessions and filtered at 200Hz with a low-pass Gaussian filter prior to quantification. Clampex software was used for all data acquisition, and Clampfit software for all data analyses (Molecular Devices, Sunnyvale, CA).

Statistics

All statistical analyses were performed using GraphPad InStat3 software (La Jolla, CA). Student's T-tests were used for pairwise comparisons, and ANOVA with appropriate post-hoc testing was used for all data sets of 3 or more comparisons. Nonparametric methods were used for data sets lacking normal distribution. Fisher's exact tests were used to analyze contingency tables for adult behavioral data. Data are shown as mean±SEM in all figures, with significance presented as $p \leq 0.05$ (*), $p \leq 0.01$ (**), $p \leq 0.001$ (***) and $p \leq 0.0001$ (****).

Acknowledgements: The pU6-BbsI-chiRNA construct was a kind gift from Melissa Harrison, Kate O'Connor-Giles and Jill Wildonger. We are very grateful to the Bloomington *Drosophila* Stock Center (Indiana University) for essential genetic stocks, and the Developmental Studies Hybridoma Bank (University of Iowa) for essential antibodies used in this study.

Competing Interests: The authors declare the absence of any commercial or financial relationships that could be possibly construed as a potential conflict of interest.

Author Contributions: W.M.P. and K.B. conceived the study and designed all experiments. W.M.P did all the genetics, CRISPR/Cas9, qRT-PCR, behavior, imaging and electrophysiology; M.D. and K.A. performed the glycomics analyses; and M.L.D. conducted all Western blots. W.M.P., C.L.G., M.T. and K.B. analyzed the data and co-wrote the manuscript.

Funding: W.M.P. was supported by F31 5F31NS084622. This work was supported by R01 MH096832 to K.B.

References

Abramoff, M.D., Magalhaes, P.J., Ram, S.J. (2001). Image Processing with ImageJ. *Biophotonics International*. 11(7), 36-42.

Altmann, F., Fabini, G., Ahorn, H., Wilson, I.B. (2001). Genetic model organisms in the study of N-glycans. *Biochimie*. 83(8), 703-12.

Andreotti, G., Cabeza de Vaca, I., Poziello, A., Monti, M.C., Guallar, V., Cubellis, M.V. (2014). Conformational response to ligand binding in phosphomannomutase2: insights into inborn glycosylation disorder. *J. Biol. Chem*. 289(50), 34900-10.

Aoki, K., Perlman, M., Lim, J.M., Cantu, R., Wells, L., Tiemeyer, M. (2007). Dynamic developmental elaboration of N-linked glycan complexity in the *Drosophila melanogaster* embryo. *J. Biol. Chem*. 282(12), 9127-42.

Ataman, B., Ashley, J., Gorczyca, D., Gorczyca, M., Mathew, D., Wichmann, C., Sigrist, S.J., Budnik, V. (2006). Nuclear trafficking of *Drosophila* Frizzled-2 during synapse development requires the PDZ protein dGRIP. *Proc Natl Acad Sci U S A*. 103(20), 7841-6.

Ataman, B., Ashley, J., Gorczyca, M., Ramachandran, P., Fouquet, W., Sigrist, S.J., Budnik, V. (2008). Rapid activity-dependent modifications in synaptic structure and function require bidirectional Wnt signaling. *Neuron*. 57(5), 705-18.

Barone, R., Fiumara, A., Jaeken, J. (2014). Congenital disorders of glycosylation with emphasis on cerebellar involvement. *Semin Neurol*. 34(3), 357-66.

Barone, R., Carrozzi, M., Parini, R., Battini, R., Martinelli, D., Elia, M., Spada, M., Lilliu, F., Ciana, G., Burlina, A., Leuzzi, V., Leoni, M., Sturiale, L., Matthijs, G., Jaeken, J., Di Rocco, M., Garozzo, D., Fiumara, A. (2015). A nationwide survey of PMM2-CDG in Italy: high frequency of a mild neurological variant associated with the L32R mutation. *J Neurol*. 262(1), 154-64.

Brand, A.H., Perrimon, N. (1993). Targeted gene expression as a means of altering cell fates and generating dominant phenotypes. *Development*. 118(2), 401-15.

Cline, A., Gao, N., Flanagan-Steet, H., Sharma, V., Rosa, S., Sonon, R., Azadi, P., Sadler, K.C., Freeze, H.H., Lehrman, M.A., Steet, R. (2012). A zebrafish model of PMM2-CDG reveals altered neurogenesis and a substrate-accumulation mechanism for N-linked glycosylation deficiency. *Mol Biol Cell*. 23(21), 4175-87.

Cylwik, B., Naklicki, M., Chrostek, L., Gruszewska, E. (2013). Congenital disorders of glycosylation. Part I. Defects of protein N-glycosylation. *Acta Biochim Pol*. 60(2), 151-61.

Dani, N., Broadie, K. (2012). Glycosylated synaptomatrix regulation of trans-synaptic signaling. *Dev Neurobiol*. 72(1), 2-21.

Dani, N., Nahm, M., Lee, S., Broadie, K. (2012). A targeted glycan-related gene screen reveals heparan sulfate proteoglycan sulfation regulates WNT and BMP trans-synaptic signaling. *PLoS Genet*. 8(11), e1003031

Dani N., Zhu H., Broadie, K. (2014). Two protein N-acetylgalactosaminyl transferases regulate synaptic plasticity by activity-dependent regulation of integrin signaling. *J Neurosci*. 34(39), 13047-65.

Dear, M.L., Dani, N., Parkinson, W., Zhou, S., Broadie, K. (2016). Two matrix metalloproteinase classes reciprocally regulate synaptogenesis. *Development* 143(1), 75-87.

Van Dijk, W., Koeleman, C., Van het Hof, B., Poland, D., Jakobs, C., Jaeken, J. (2001). Increased alpha3-fucosylation of alpha(1)-acid glycoprotein in patients with congenital disorder of glycosylation type IA (CDG-Ia). *FEBS Lett.* 494(3), 232-5.

Freeze, H.H., Chong, J.X., Bamshad, M.J., Ng, B.G. (2014). Solving glycosylation disorders: fundamental approaches reveal complicated pathways. *Am J Hum Genet*. 94(2), 161-75.

Freeze, H.H., Eklund, E.A., Ng, B.G., Patterson, M.C. (2015). Neurological Aspects of Human Glycosylation Disorders. *Annu Rev Neurosci*. 38, 105-25.

Gao, N., Shang, J., Huynh, D., Manthati, V.L., Aria,s C., Harding, H.P., Kaufman, R.J., Mohr, I., Ron, D., Falck, J.R., Lehrman, M.A. (2011). Mannose-6-phosphate regulates destruction of lipid-linked oligosaccharides. *Mol Biol Cell*. 22(17), 2994-3009.

Gatto, C.L., and Broadie, K. (2011). *Drosophila* modeling of heritable neurodevelopmental disorders. *Curr Opin Neurobiol.* 21(6), 834-41.

Gjorgjieva, J., Berni, J., Evers, J.F., Eglen, S.J. (2013). Neural circuits for peristaltic wave propagation in crawling *Drosophila* larvae: analysis and modeling. *Front Comput Neuro*. 7, 24.

Glasheen, B.M., Kabra, A.T., Page-McCaw, A. (2009). Distinct functions for the catalytic and hemopexin domains of *Drosophila* matrix metalloproteinase. *Pro Nat Acad Sci* 106(8), 2659-64.

Glasheen, B.M., Robbins, R.M., Piette, C., Beitel, G.J., Page-McCaw, A. (2010). A matrix metalloproteinase mediates airway remodeling in *Drosophila*. *Dev Biol*. 344(2), 772-83.

Godenschwege, T.A., Pohar, N., Buchner, S., Buchner, E. (2000). Inflated wings, tissue autolysis and early death in tissue inhibitor of metalloproteinases mutants of *Drosophila*. *Eur J Cell Biol*. 79(7), 495-501.

Gratz, S.J., Cummings, A.M., Nguyen, J.N., Hamm,, D.C., Donohue, L.K., Harrison, M.M., Wildonger, J., O'Connor-Giles, K.M. (2013). Genome engineering of *Drosophila* with the CRISPR RNA-guided Cas9 nuclease. *Genetics*. 194(4), 1029-35.

Grünewald, S. (2009). The clinical spectrum of phosphomannomutase 2 deficiency (CDG-Ia). *Biochim Biophys Acta*. 1792(9), 827-34.

Haeuptle, M.A., Hennet, T. (2009). Congenital disorders of glycosylation: an update on defects affecting the biosynthesis of dolichol-linked oligosaccharides. *Hum Mutat*. 30(12), 1628-41.

ten Hagen, K.G., Zhang, L., Tian, E., Zhang, Y. (2009). Glycobiology on the fly: developmental and mechanistic insights from *Drosophila*. *Glycobiology*. (2), 102-11.

Himmelreich, N., Kaufmann, L.T., Steinbeisser, H., Körner, C., Thiel, C.J. (2015). Lack of phosphomannomutase 2 affects Xenopus laevis morphogenesis and the non-canonical Wnt5a/Ror2 signalling. *Inherit Metab Dis*. 38(6), 1137-46.

Jaeken, J., Vanderschueren-Lodeweyckx, M., Casaer, P., Snoeck, L., Corbeel, L., Eggermont, E., Eeckels, R. (1980). Familial psychomotor retardation with markedly fluctuating serum prolactin, FSH and GH levels, partial TBG-deficiency, increased serum arylsulfatase-A and increased CSF protein- new syndrome? *Pediatr Res*. 14:179

Jaeken J. (2010). Congenital disorders of glycosylation. *Ann N Y Acad Sci*. 1214, 190-8.

Jaeken, J. (2013). Congenital disorders of glycosylation. *Handb Clin Neurol.* 113, 1737-43.

Jia, Q., Liu, Y., Liu, H., Li, S. (2014). Mmp1 and Mmp2 cooperatively induce Drosophila fat body cell dissociation with distinct roles. *Sci Rep*. 4:7535.

Jumbo-Lucioni P, Parkinson W, Broadie K. (2014). Overelaborated synaptic architecture and reduced synaptomatrix glycosylation in a *Drosophila* classic galactosemia disease model. *Dis Model Mech*. 7(12), 1365-78.

Katoh, T., Takase, J., Tani, Y., Amamoto, R., Aoshima, N., Tiemeyer, M., Yamamoto, K., Ashida, H. (2013). Deficiency of α-glucosidase I alters glycoprotein glycosylation and lifespan in *Caenorhabditis elegans*. *Glycobiology*. 23(10), 1142-51.

Katoh, T., Tiemeyer, M. (2013). The N's and O's of *Drosophila* glycoprotein glycobiology. *Glycoconj J*. 30(1), 57-66.

Kerr, K.S., Fuentes-Medel, Y., Brewer, C., Barria, R., Ashley, J., Abruzzi, K.C., Sheehan, A., Tasdemir-Yilmaz, O.E., Freeman, M.R., Budnik, V. (2014). Glial wingless/Wnt regulates glutamate receptor clustering and synaptic physiology at the *Drosophila* neuromuscular junction. *J Neurosci*. 34(8), 2910-20.

Kessenbrock, K., Plaks, V., Werb, Z. (2010). Matrix metalloproteinases: regulators of the tumor microenvironment. *Cell*. 141(1), 52-67.

Kjaergaard, S., Kristiansson, B., Stibler, H., Freeze, H.H., Schwartz, M., Martinsson, T., Skovby, F. (1998). Failure of short-term mannose therapy of patients with carbohydrate-deficient glycoprotein syndrome type 1A. *Acta Paediatr.* 87(8), 884-8.

Kohsaka, H., Takasu, E., Morimoto, T., Nose, A. (2014). A group of segmental premotor neurons regulates speed of axial locomotion in *Drosophila* larvae. *Curr Biol.* 24(22), 2632-42.

Koles, K., Lim, J.M., Aoki, K., Porterfield, M., Tiemeyer, M., Wells, L., Panin, V. (2007). Identification of N-glycosylated proteins from the central nervous system of *Drosophila melanogaster*. *Glycobiology*. 17(12), 1388-403.

Kurosaka, A., Yano, A., Itoh, N., Kuroda, Y., Nakagawa, T., Kawasaki, T. (1991). The structure of a neural specific carbohydrate epitope of horseradish peroxidase recognized by anti-horseradish peroxidase antiserum. *J Biol Chem.* 266(7), 4168-72.

Llano, E., Adam, G., Pendás, A.M., Quesada, V., Sánchez, L.M., Santamariá, I., Noselli, S., López-Otín, C. (2002). Structural and enzymatic characterization of *Drosophila* Dm2-MMP, a membrane-bound matrix metalloproteinase with tissue-specific expression. *J Biol Chem*. 277(26), 23321-9.

Llano, E., Pendás, A.M., Aza-Blanc, P., Kornberg, T.B., López-Otín, C. (2000). Dm1-MMP, a matrix metalloproteinase from *Drosophila* with a potential role in extracellular matrix remodeling during neural development. *J Biol Chem*. 275(46), 35978-85.

Lin, D.M., Goodman, C.S. (1994). Ectopic and increased expression of Fasciclin II alters motoneuron growth cone guidance. *Neuron*. 13(3), 507-23.

de Lonlay, P., Seta, N., Barrot, S., Chabrol, B., Drouin, V., Gabriel, B.M., Journel, H., Kretz, M., Laurent, J., Le Merrer, M., Leroy, A., Pedespan, D., Sarda, P., Villeneuve, N., Schmitz, J., van Schaftingen, E., Matthijs, G., Jaeken, J., Korner, C., Munnich, A., Saudubray, J.M., Cormier-Daire, V. (2001). A broad spectrum of clinical presentations in congenital disorders of glycosylation I: a series of 26 cases. *J Med Genet*. 38(1), 14-9.

Mair, W., Piper, M.D., Partridge, L. (2005). Calories do not explain extension of life span by dietary restriction in Drosophila. *PLoS Biol*. 3(7):e223.

Marquardt, T., Denecke, J. (2003). Congenital disorders of glycosylation: review of their molecular bases, clinical presentations and specific therapies. *Eur J Pediatr.* 162(6), 359-79.

Martin, P.T. (2003). Glycobiology of the neuromuscular junction. *J Neurocyt*. 32(5-8), 915-29.

Mathew, D., Ataman, B., Chen, J., Zhang, Y., Cumberledge, S., Budnik, V. (2005). Wingless signaling at synapses is through cleavage and nuclear import of receptor DFrizzled2. *Science*. 310(5752), 1344-7.

Matthijs, G., Schollen, E., Van Schaftingen, E., Cassiman, J.J., Jaeken, J. (1998). Lack of homozygotes for the most frequent disease allele in carbohydrate-deficient glycoprotein syndrome type 1A. *Am J Hum Genet*. 62(3), 542-50.

Min, K.J., Tatar, M. (2006) Restriction of amino acids extends lifespan in *Drosophila melanogaster*. *Mech Ageing Dev*. 127(7), 643-6.

Mayatepek, E., Kohlmüller, D. (1998). Mannose supplementation in carbohydrate-deficient glycoprotein syndrome type I and phosphomannomutase deficiency. *Eur J Ped.* 157(7), 605-6.

Monin, M.L., Mignot, C., De Lonlay, P., Héron, B., Masurel, A., Mathieu-Dramard, M., Lenaerts, C., Thauvin, C., Gérard, M., Roze, E., Jacquette, A., Charles, P., de Baracé, C., Drouin-Garraud, V., Khau Van Kien, P., Cormier-Daire, V., Mayer, M., Ogier, H.,

Brice, A., Seta, N., Héron, D. (2014). 29 French adult patients with PMM2-congenital disorder of glycosylation: outcome of the classical pediatric phenotype and depiction of a late-onset phenotype. *Orphanet J Rare Dis*. 11, 9:207.

de la Morena-Barrio, M.E., Hernández-Caselles, T., Corral, J., García-López, R., Martínez-Martínez, I., Pérez-Dueñas, B., Altisent, C., Sevivas, T., Kristensen, S.R., Guillén-Navarro, E., Miñano, A., Vicente, V., Jaeken, J., Lozano, M.L. (2013). GPI-anchor and GPI-anchored protein expression in PMM2-CDG patients. *Orphanet J Rare Dis*. 8, 170.

Müller, D., Jagla, T., Bodart, L.M., Jährling, N., Dodt, H.U., Jagla, K., Frasch, M. (2010). Regulation and functions of the lms homeobox gene during development of embryonic lateral transverse muscles and direct flight muscles in *Drosophila*. *PLoS One*. 5(12), e14323.

Nichols, C. D., Becnel, J., Pandey, U. B. (2012). Methods to Assay *Drosophila* Behavior. *J. Vis. Exp.* (61), e3795.

Packard, M., Koo, E.S., Gorczyca, M., Sharpe, J., Cumberledge, S., Budnik, V. (2002). The *Drosophila* Wnt, wingless, provides an essential signal for pre- and postsynaptic differentiation. *Cell*. 111(3), 319-30.

Page-McCaw, A., Ewald, A.J., Werb, Z. (2007). Matrix metalloproteinases and the regulation of tissue remodelling. *Nat Rev Mol Cell Biol*. 8(3), 221-33.

Parkinson, W., Dear, M.L., Rushton, E., Broadie, K. (2013). N-glycosylation requirements in neuromuscular synaptogenesis. *Development*. 2013 140(24), 4970-81.

Pohar, N., Godenschwege, T.A., Buchner, E. (1999). Invertebrate tissue inhibitor of metalloproteinase: structure and nested gene organization within the synapsin locus is conserved from Drosophila to human. *Genomics*. 57(2), 293-6.

Reiter, L.T., Potocki, L., Chien, S., Gribskov, M., Bier, E. (2001). A systematic analysis of human disease-associated gene sequences in *Drosophila*. *Genome Res*. 11(6), 1114-25.

Ristow, M., Schmeisser, S. (2011) Extending life span by increasing oxidative stress. *Free Radic Biol Med.* 51(2), 327-36.

Rohrbough, J., Rushton, E., Woodruff, E. 3rd., Fergestad, T., Vigneswaran, K., Broadie, K. (2007). Presynaptic establishment of the synaptic cleft extracellular matrix is required for post-synaptic differentiation. *Genes Dev*. 21(20), 2607-28.

Rushton, E., Rohrbough, J., Deutsch, K., Broadie, K. (2012). Structure-function analysis of endogenous lectin mind-the-gap in synaptogenesis. *Dev Neurobiol*. 72(8), 1161-79.

Sarkar, M., Leventis, P.A., Silvescu, C.I., Reinhold, V.N., Schachter, H., Boulianne, G.L. (2006). Null mutations in Drosophila N-acetylglucosaminyltransferase I produce defects in locomotion and a reduced life span. *J Biol Chem*. 281(18), 12776-85.

Schneider, A., Thiel, C., Rindermann, J., DeRossi, C., Popovici, D., Hoffmann, G.F.,

Gröne, H.J., Körner, C. (2011). Successful prenatal mannose treatment for congenital disorder of glycosylation-Ia in mice. *Nat Med*. 18(1), 71-3.

Schulte-Merker, S., and Stainier, D.Y. (2014). Out with the old, in with the new: reassessing morpholino knockdowns in light of genome editing technology. *Development*. 141(16), 3103-4.

Scott, H., Panin, V.M. (2014a). N-glycosylation in regulation of the nervous system. *Adv Neurobiol*. 9, 367-94.

Scott H, Panin VM. (2014b). The role of protein N-glycosylation in neural transmission. *Glycobiology*. 24(5), 407-17.

Seppo, A., Tiemeyer, M. (2000). Function and structure of Drosophila glycans. *Glycobiology*. 10(8), 751-60.

Sharma, V., Ichikawa, M., He, P., Scott, D.A., Bravo, Y., Dahl, R., Ng, B.G., Cosford, N.D., Freeze, H.H. (2011). Phosphomannose isomerase inhibitors improve N-glycosylation in selected phosphomannomutase-deficient fibroblasts. *J Biol Chem.* 286(45), 39431-8.

Silvaggi, N.R., Zhang, C., Lu, Z., Dai, J., Dunaway-Mariano, D., Allen, K.N. (2006). The X-ray crystal structures of human alpha-phosphomannomutase 1 reveal the structural basis of congenital disorder of glycosylation type 1a. *J Biol Chem*. 281(21), 14918-26.

Speese, S.D., Ashley, J., Jokhi, V., Nunnari, J., Barria, R., Li, Y., Ataman, B., Koon, A.,

Chang, Y.T., Li, Q., Moore, M.J., Budnik, V. (2012). Nuclear envelope budding enables large ribonucleoprotein particle export during synaptic Wnt signaling. *Cell.* 149(4), 832-46.

Sokolowski, M.B. (1980). Foraging strategies of *Drosophila melanogaster*: a chromosomal analysis. *Behav Genet*. 10(3), 291-302.

Song, W., Henquet, M.G., Mentink, R.A., van Dijk, A.J., Cordewener, J.H., Bosch, D., America, A.H., van der Krol, A.R. (2011). N-glycoproteomics in plants: perspectives and challenges. *J Proteomics*. 74(8), 1463-74.

Stanley, P., Schachter, H., Taniguchi, N. (2009). N-Glycans. In: *Essentials of Glycobiology*. (ed. A. Varki, R.D. Cummings, J.D. Esko, H.H. Freeze, P. Stanley, C.R. Bertozzi, G.W. Hart, M.E. Etzler), pp. 101-114. Cold Spring Harbor (NY): Cold Spring Harbor Laboratory Press.

Stefanits, H., Konstantopoulou, V., Kuess, M., Milenkovic, I., Matula, C. (2014). Initial diagnosis of the congenital disorder of glycosylation PMM2-CDG (CDG1a) in a 4-year-old girl after neurosurgical intervention for cerebral hemorrhage. *J Neurosurg Pediatr*. 14(5), 546-9.

Sternlicht, M.D. and Werb, Z. (2001). How Matrix metalloproteinases regulate cell behavior. *Annu Rev Cell Biol*. 17, 463–516.

Thiel, C., Lübke, T., Matthijs, G., von Figura, K., Körner, C. (2006). Targeted disruption of mouse phosphomannomutase 2 causes early embryonic lethality. *Mol Cell Biol*. 26(15),

5615-20.

Thiel, C., Körner, C. (2013). Therapies and therapeutic approaches in Congenital Disorders of Glycosylation. *Glycoconj J*. 30(1), 77-84.

Thiel, C., Meßner-Schmitt, D., Hoffmann, G.F., Körner, C. (2013). Screening for congenital disorders of glycosylation in the first weeks of life. *J Inherit Metab Dis*. 36(5), 887-92.

Wang, X., Page-McCaw, A. (2014). A matrix metalloproteinase mediates long-distance attenuation of stem cell proliferation. *J Cell Biol*. 206(7), 923-36.

Varki, A., Sharon, N. (2009). Historical background and overview. In: *Essentials of Glycobiology*. (ed. A. Varki, R.D. Cummings, J.D. Esko, H.H. Freeze, P. Stanley, C.R. Bertozzi, G.W. Hart, M.E. Etzler), pp. 1-22. Cold Spring Harbor (NY): Cold Spring Harbor Lab Press.

Vleugels, W., Duvet, S., Peanne, R., Mir, A.M., Cacan, R., Michalski, J.C., Matthijs, G., Foulquier, F. (2011). Identification of phosphorylated oligosaccharides in cells of patients with a congenital disorders of glycosylation (CDG-I). *Biochimie*. 93(5), 823-33.

Yuste-Checa, P., Gámez, A., Brasil, S., Desviat, L.R., Ugarte, M., Pérez-Cerdá, C., Pérez, B. (2015). The Effects of PMM2-CDG-Causing Mutations on the Folding, Activity, and Stability of the PMM2 Protein. *Hum Mutat*. 36(9), 851-60.

Zaffran, S., Astier, M., Gratecos, D., Sémériva, M. (1997). The held out wings (how) Drosophila gene encodes a putative RNA-binding protein involved in the control of muscular and cardiac activity. *Development*. 124(10), 2087-98.

Zhang, L., Ward, R.E. (2009). *uninflatable* encodes a novel ectodermal apical surface protein required for tracheal inflation in Drosophila. *Dev Biol*. 336(2), 201-12.

Figures

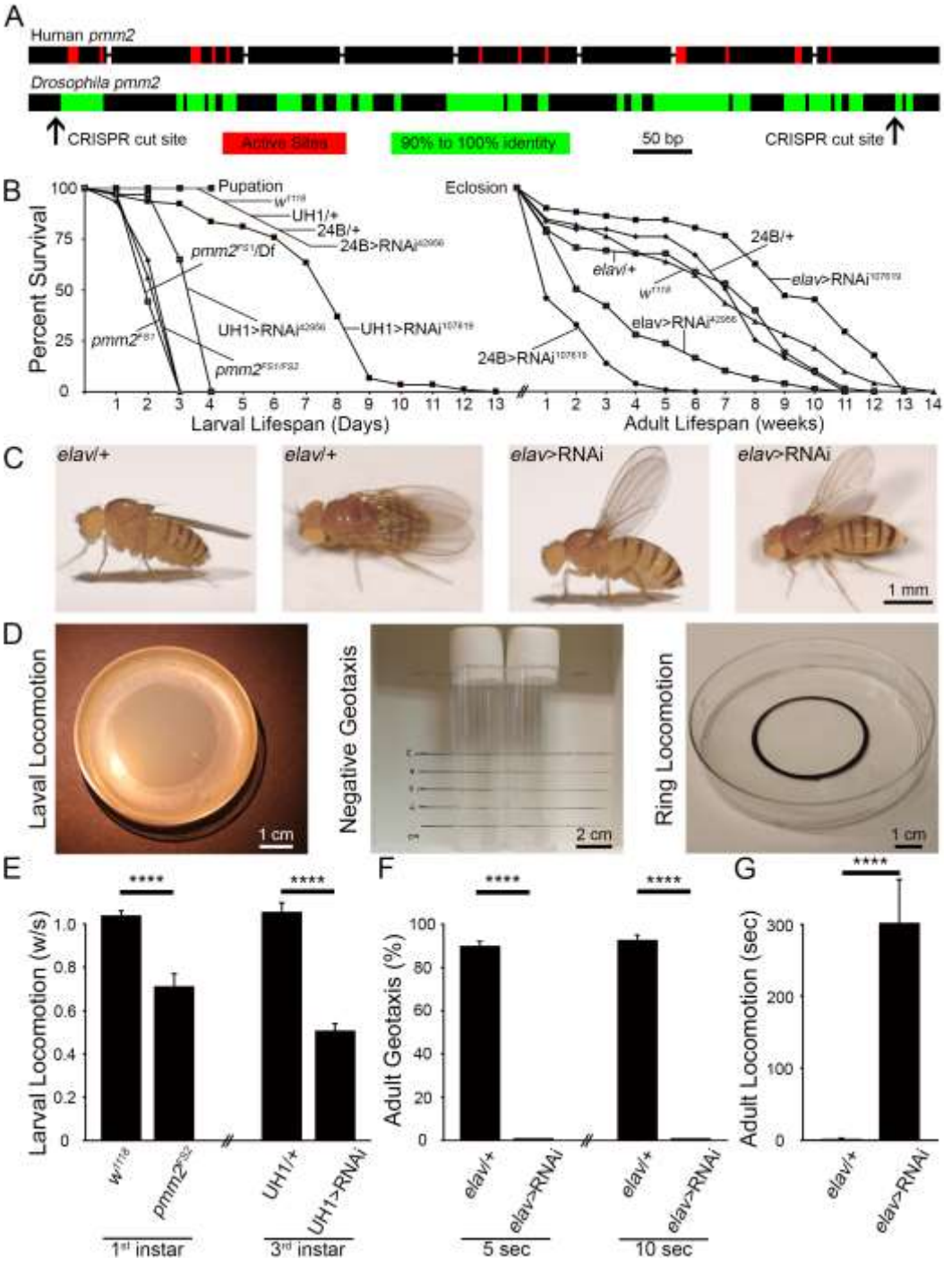

Figure 1: *Drosophila* PMM2 levels determine lifespan and coordinated movement ability.

A) Comparison of human and *Drosophila pmm2* genes. Human *pmm2* contains 8 exons (black boxes) compared to the single reading frame in *Drosophila*. Highly conserved active sites (red) and other regions of high identity (90-100%, green) are depicted. CRISPR-generated null mutants were made at both 5' and 3' ends of *pmm2* (arrows). **B)** Larval lifespan of null mutants ($pmm2^{FS1}$, $pmm2^{FS1}$/Df and heteroallelic $pmm2^{FS1/FS2}$), and two driven RNAi lines ($RNAi^{42956}$ and $RNAi^{107619}$) compared to controls (left). Adult lifespan with targeted neural (*elav*-Gal4) and muscle (24B-Gal4) *pmm2* RNAi compared to controls (right). **C)** Examples of wing posture with neural *pmm2* RNAi. **D)** Behavioral assays: larval locomotion on apple juice plates towards edge yeast attractant (left); adult negative geotaxis climbing to 2 cm height (middle), and adult horizontal locomotion for flies with wings removed exiting a 4 cm ring (right). **E)** Normalized quantification of 1st (left) and 3rd instar (right) larval locomotion (peristaltic waves/second) in genotypes shown. **F)** Quantification of adult negative geotaxis as percent animals climbing to 2cm height at 5 (left) and 10 (right) seconds. **G)** Quantification of adult horizontal locomotion as time to exit 4cm ring). Significance: $p<0.0001$ (****). Sample sizes: $n\geq17$ animals/genotype.

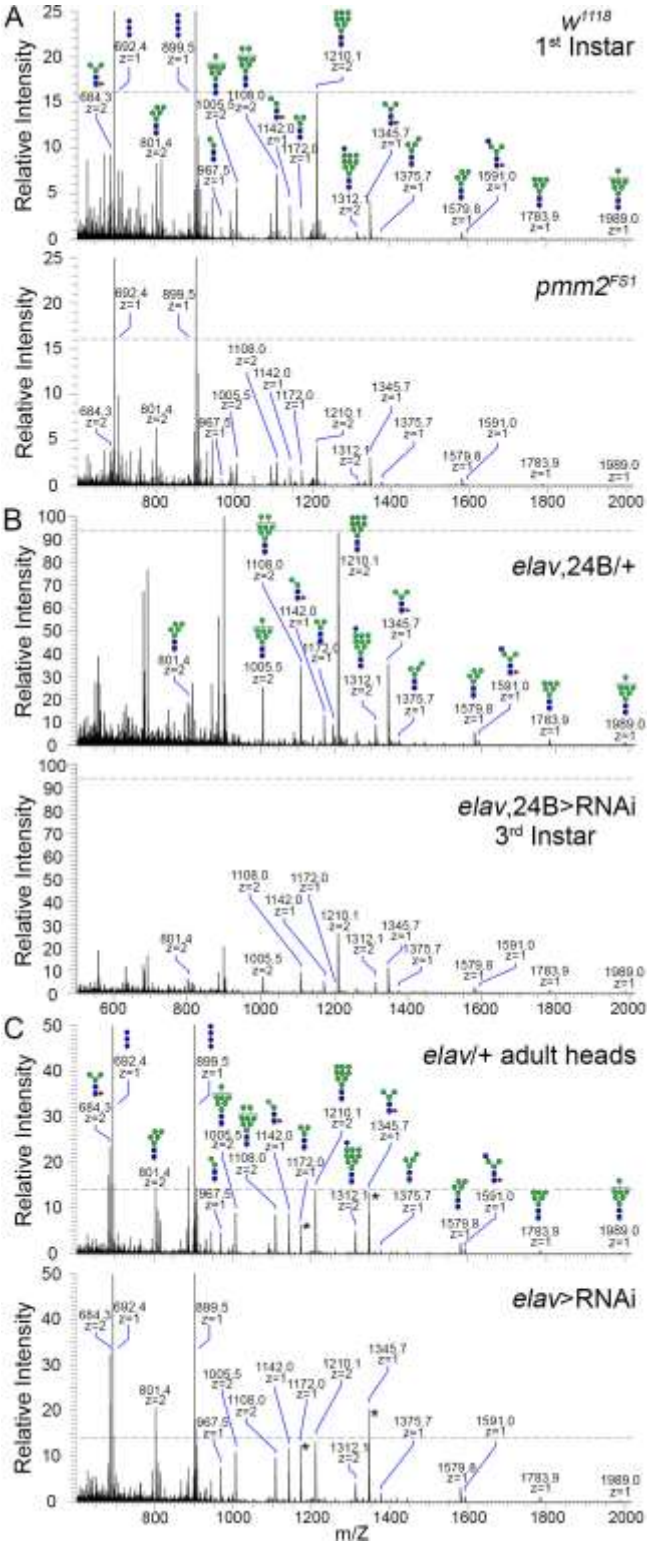

Figure 2: PMM2 loss dramatically alters N-linked glycoprotein glycosylation.

Full mass spectrometry (MS) spectra for permethylated glycans harvested from **(A)** age-matched w^{1118} genetic control (top) and $pmm2^{FS1}$ null (bottom) 1st instars, **(B)** *elav*-Gal4,24B-Gal4/+ transgenic control (top) and *elav*-Gal4,24B-Gal4>RNAi^{42956} (bottom) 3rd instars, and **(C)** *elav*-Gal4/+ transgenic control (top) and *elav*-Gal4>RNAi^{42956} (bottom) adult heads. Dashed lines indicate the relative abundance of $Man_9GlcNAc_2$ (m/z=1210.1, doubly-charged) in each control for comparison with mutants across genotypes. In all panels, mass peaks at m/z=692.4 and 899.5 are Hex_3 and Hex_4 glycans spiked into samples as external calibration standards. The cartoon representations of glycan structures are shown in accordance with glycomics community conventions (Varki and Sharon, 2009).

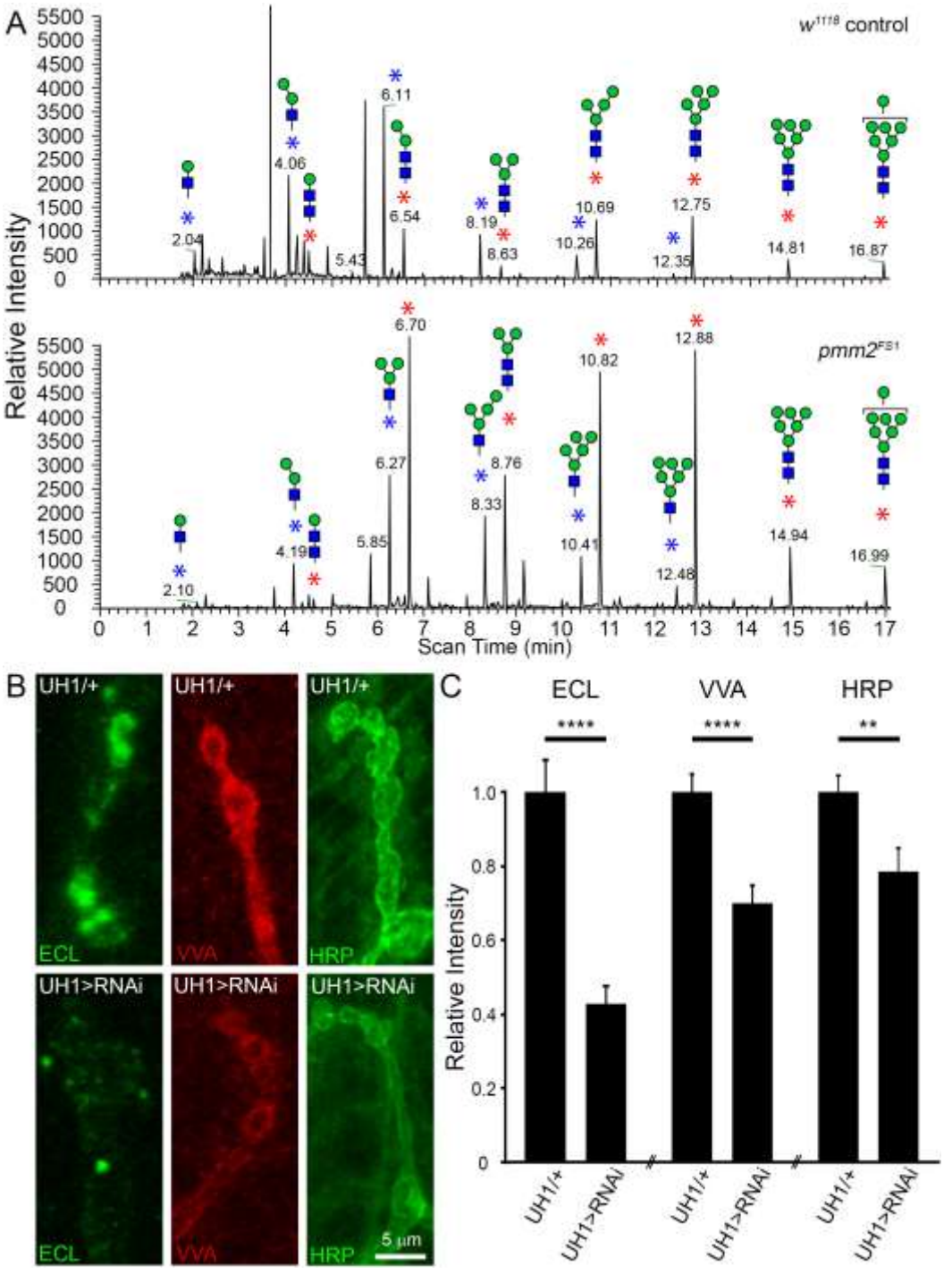

Figure 3: PMM2 loss increases FOS and reduces NMJ N-linked glycoprotein glycosylation.

A) Free oligosaccharides (FOS) from w^{1118} genetic control and $pmm2^{FS1}$ null 1st instar larvae. FOS detected as products of sequential PNGase and endo-N-acetylglucosaminidase digestion (N1, blue asterisks), or as glycans with 2 reducing terminal GlcNAc residues (N2, red asterisks). Total ion mapping chromatograms filtered for loss of non-reducing terminal HexNAc residues to show the two FOS classes. **B)** Representative images of *Erythrina cristagalli* (ECL, green; left), *Vicia villosa* (VVA, red; middle) and horse radish peroxidase (HRP, green; right) NMJ labeling in *pmm2* knockdowns (bottom) compared to transgenic controls (top). **C)** Quantification of fluorescent labeling intensity in UH1-Gal4/+ transgenic control vs. UH1-Gal4>RNAi^{107619}. Significance: $p \leq 0.01$ (**), $p \leq 0.0001$ (****). Sample sizes: $n \geq 24$ NMJs/12 animals per genotype.

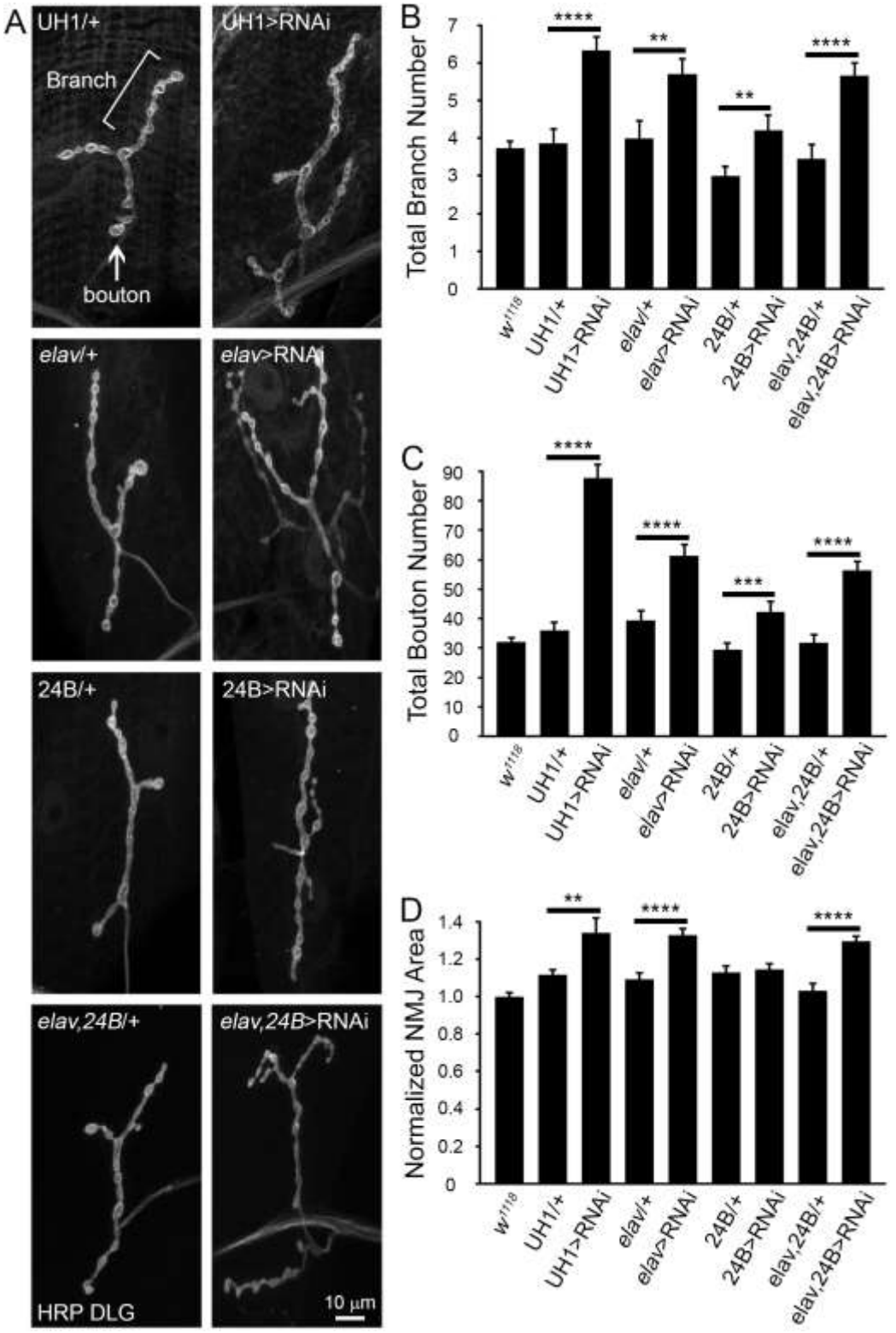

Figure 4: PMM2 loss results in striking NMJ synaptic structural overgrowth.

A) Representative wandering 3rd instar muscle 4 NMJ images of ubiquitous (UH1, top), neural (*elav*, second), muscle (24B, third) and double (*elav*, 24B, bottom) driver controls (left column), compared to RNAi-mediated *pmm2* knockdown (right). NMJs are co-labeled for presynaptic HRP and postsynaptic DLG, merged and shown in black-and-white to best illustrate structure. Quantification of NMJ branch number **(B)**, bouton number **(C)** and terminal area **(D)** in the above 8 genotypes compared to w^{1118} (9 genotypes total). Significance: $p \leq 0.01$ (**), $p \leq 0.001$ (***), $p \leq 0.0001$ (****). Sample sizes: $n \geq 22$ NMJs/12 animals for each genotype.

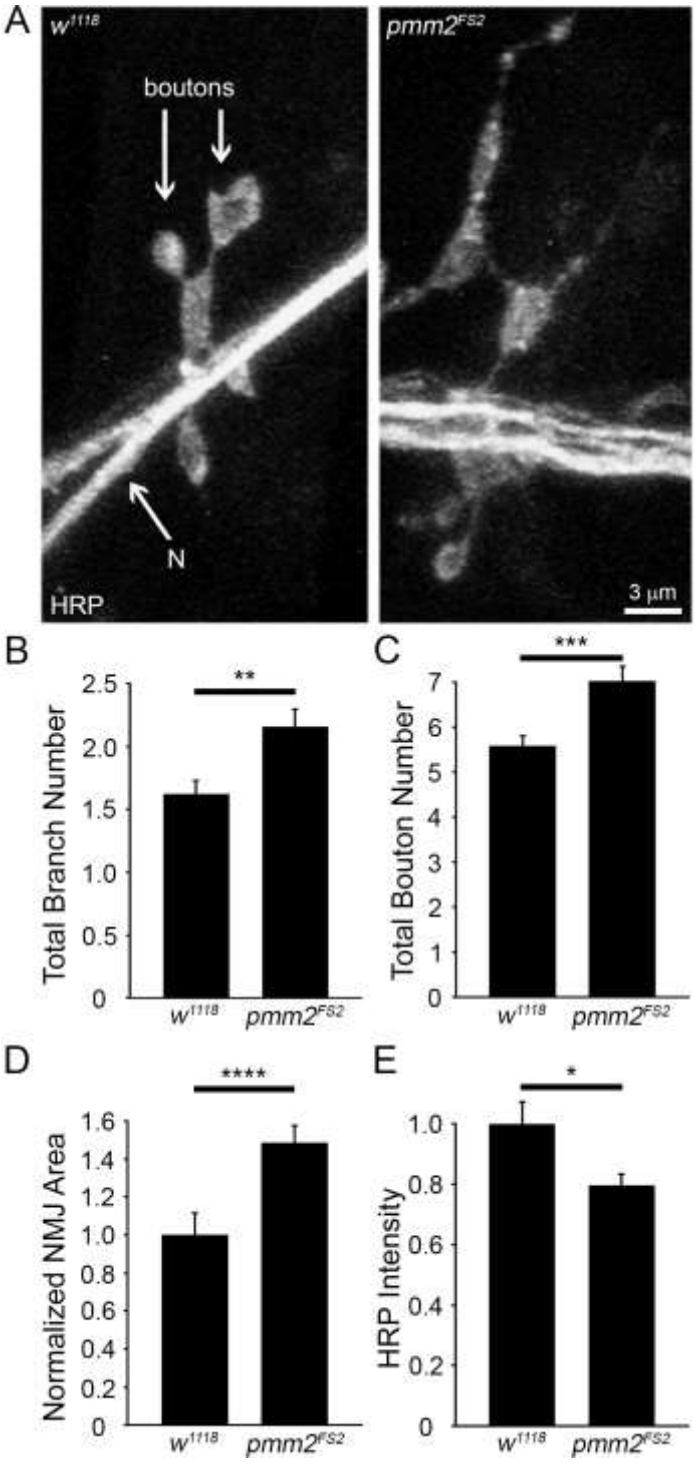

Figure 5: Early lethal *pmm2* null mutants exhibit NMJ overgrowth and loss of N-glycans.

A) Representative 1st instar muscle 4 NMJ images from genetic background control (w^{1118}, left) and *pmm2* null mutant ($pmm2^{FS2}$, right). NMJs are labeled for the presynaptic anti-HRP. Quantification of synaptic branch number **(B)**, bouton number **(C)**, synaptic terminal area **(D)** and HRP fluorescence labeling intensity **(E)**. Significance: $p \leq 0.05$ (*), $p \leq 0.01$ (**), $p \leq 0.001$ (***) and $p < 0.0001$ (****). Sample sizes: $n \geq 30$ NMJs/13 animals per genotype.

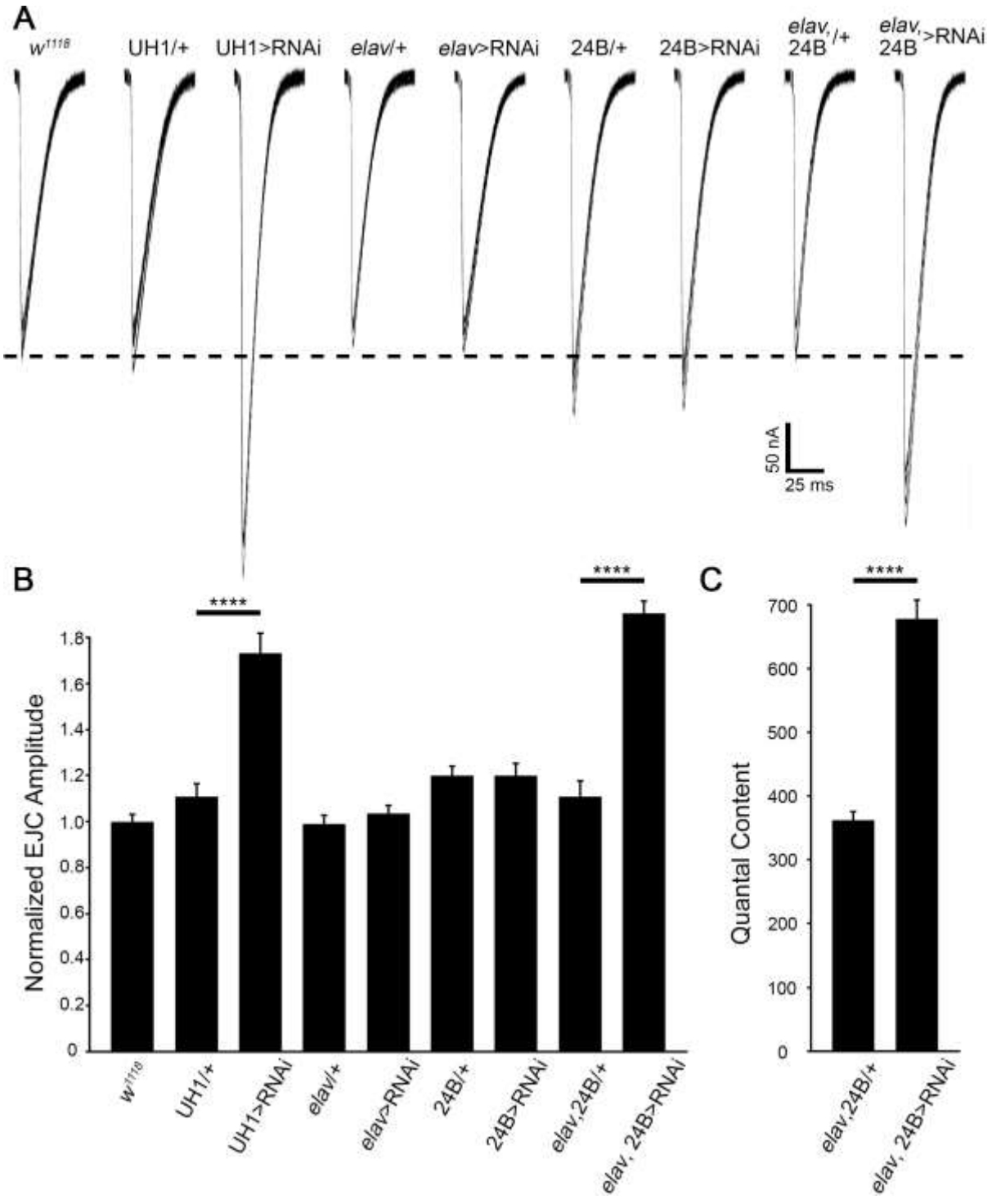

Figure 6: Coupled pre- and postsynaptic PMM2 removal increases neurotransmission.

A) Representative two-electrode voltage-clamp (TEVC) recordings of nerve-stimulation evoked excitatory junctional currents (EJCs) from wandering 3rd instar muscle 6. Superimposed traces are shown in response to nerve stimulation at 1.0mM Ca^{2+} comparing UH1-Gal4>RNAi^{107619}, *elav*-Gal4>RNAi^{42956}, 24B-Gal4>RNAi^{42956} and *elav*-Gal4, 24B-Gal4>RNAi^{42956} to w^{1118} and Gal4 diver alone controls. Quantification of peak EJC amplitude normalized to w^{1118} **(B)** and neurotransmission quantal content **(C)** Significance: $p \leq 0.0001$ (****). Sample sizes: $n \geq 16$ NMJs/8 animals per genotype.

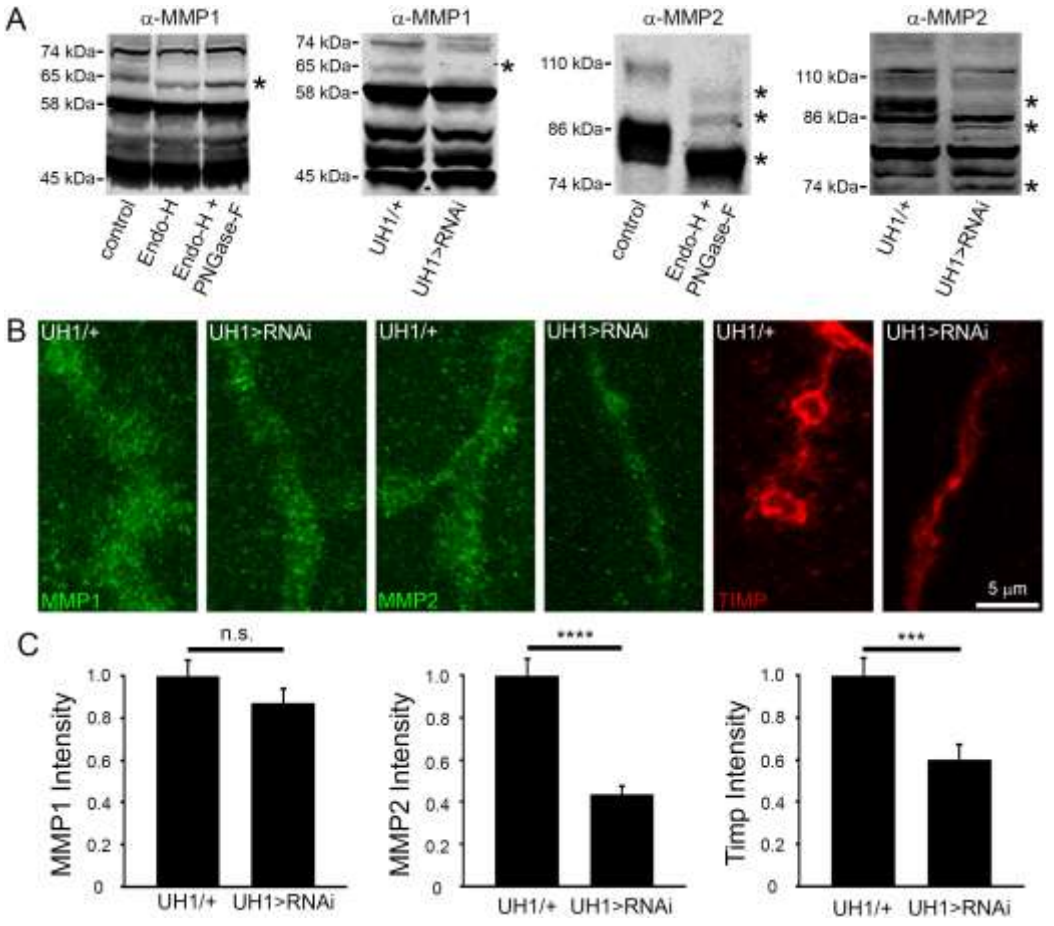

Figure 7: Loss of PMM2 down-regulates the synaptic matrix proteinase pathway.

A) Representative Western blots for MMP1 (left) and MMP2 (right); 1) with/without PNGaseF and EndoH enzymatic treatment to remove glycosylation, and 2) in UH1-Gal4/+ transgenic control and UH>RNAi^{107619} PMM2 knockdown conditions. The asterisks denote shifted bands. **B)** Representative NMJ images for anti-MMP1 (green, left), anti-MMP2 (green, center) and anti-TIMP (red, right) in UH1-Gal4/+ controls and UH1-Gal4>RNAi^{107619}. **C)** Normalized quantification of fluorescent intensities for all three proteins. Significance: $p \leq 0.001$ (***), $p \leq 0.0001$ (****) and not significant (n.s.). Sample sizes: $n \geq 20$ NMJs/12 animals per genotype.

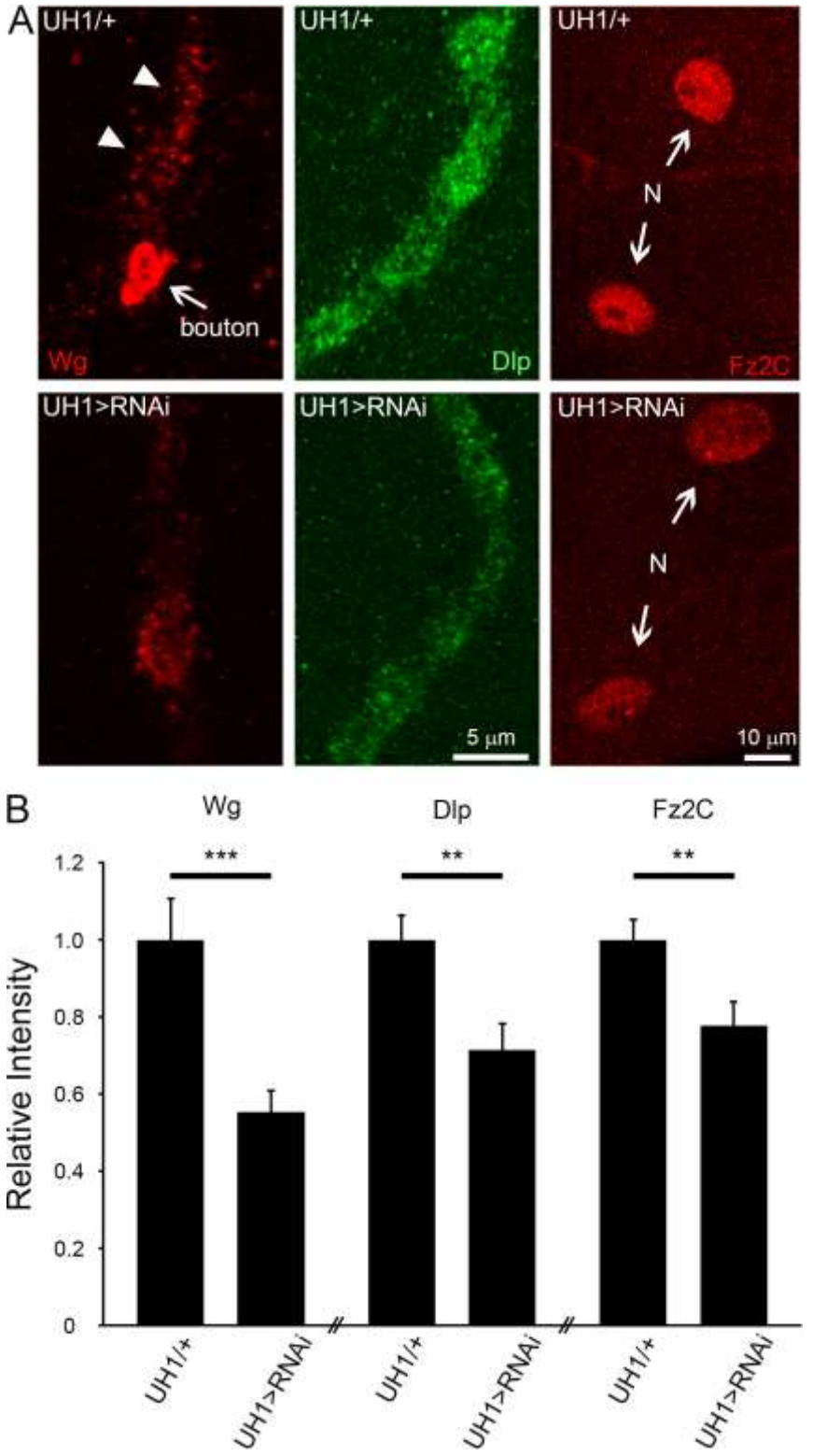

Figure 8: Loss of PMM2 down-regulates the *trans*-synaptic Wnt signaling pathway.

A) Representative NMJ images for anti-Wg (red, left), anti-Dlp (green, middle) and anti-Fz2C (red, right) in UH1-Gal4/+ controls (top) and UH1-Gal4>RNAi^{107619} (bottom). Left: Arrow indicates high Wg-expressing bouton, and arrowheads show low Wg-expressing boutons in control NMJ. Right: The arrows indicate two postsynaptic nuclei in control and mutant muscle. **B)** Normalized quantification of Wg, Dlp and Fz2C fluorescent labeling intensities. Significance: $p \leq 0.01$ (**) and $p \leq 0.001$ (***). Sample sizes: $n \geq 24$ NMJs or nuclei/12 animals per genotype.

Translational Impact

1) *Clinical Issue*: The rapidly expanding congenital disorders of glycosylation (CDG) disease family results from mutation of genes encoding glycosylation pathway proteins, which drive the addition of carbohydrate moieties to proteins. The most common CDG, CDG-Ia or PMM2-CDG, is caused by loss of phosphomannomutase type 2 (PMM2), which converts mannose-6-phosphate into mannose-1-phosphate. This obligatory step is required for all N-linked glycosylation, an important and widespread glycan modification of extracellular proteins, which aids in many aspects of protein localization and function. Human CDG-Ia patients present with severe neurological impairments, including loss of coordinated movement and intellectual disability, and are often concomitantly afflicted with multi-organ dysfunction, infection and injury also contributing to reduced lifespan. Here, we generate the first *Drosophila* CDG-Ia disease model, showing phenotypes that strongly parallel patient neurological symptoms and compromised longevity. Previous animal models have revealed important aspects of CDG-Ia disease progression in neurodevelopment and cellular signaling, but are limited by the inability to study tissue-specific reduction of PMM2 function in a temporally and spatially-controlled manner. These capacities are provided in this *Drosophila* disease model, which allows assessment of developmental, cell type-specific PMM2 involvement.
2) *Results*: The new *Drosophila* PMM2-CDG disease model recapitulates the characteristic phenotypes of the human disease state. Using both *pmm2* null mutants and targeted RNAi knockdown, we demonstrate early lethality, severe loss of coordinately movement and reduced/dysregulated glycosylation. We focus on the neuromuscular junction (NMJ) that drives movement to reveal reduced levels of synaptic glycosylation coupled to structural overelaboration and functional

strengthening. Based on phenotypes, we hypothesized that compromised NMJ synaptic glycosylation would alter matrix metalloproteinase (MMP) pathways known to modulate Wnt intercellular signaling. In testing this hypothesis, we discovered depressed MMP expression at the NMJ resulting in reduced Wnt Wingless (Wg) *trans*-synaptic signaling that modulates synaptic development and function.

3) *Implications and future directions*: Increasing evidence highlights the importance of glycosylation in neural development and function. The majority of CDG patients present with severe neurological symptoms; however, the causes remain very poorly understood. Here, we present a new *Drosophila* CDG-Ia model identifying a range of phenotypes that closely resemble human patient symptoms. This new model will allow in-depth studies to discover underlying causative mechanisms, decipher them, and ultimately inform drug design. The MMP and Wnt changes identified here represent candidate drug targets for treating CDG-Ia neurological symptoms. Discoveries aided by the relative high speed of *Drosophila* studies combined with the powerful, ever-expanding *Drosophila* genetic toolkit will open up new avenues for CDG-Ia therapeutic intervention.